UNIVERSITY OF OKLAHOMA
GRADUATE COLLEGE
School of Geosciences

SEISMIC-BASED CHARACTERIZATION OF A CARBONATE GAS STORAGE RESERVOIR ASSISTED BY MACHINE LEARNING TECHNIQUES

A THESIS
SUBMITTED TO THE GRADUATE FACULTY
In partial fulfillment of the requirements for the
Degree of
MASTER OF SCIENCE

By
CLAYTON SILVER
Norman, Oklahoma
2021

SEISMIC-BASED CHARACTERIZATION OF A CARBONATE GAS STORAGE RESERVOIR ASSISTED BY MACHINE LEARNING TECHNIQUES

A THESIS APPROVED FOR THE

SCHOOL OF GEOSCIENCES

BY THE COMMITTEE CONSISTING OF

Dr. Heather Bedle

Dr. Matthew Pranter

Dr. Matthew Rine

Acknowledgments

This thesis is dedicated to my loving family, fiancé, and Dr. Bedle. I could not have done it without all of the support I have received from you all over the years, and constant motivation to continue my education. Mom, Dad, Brandon and Jackson – Thank you for your support to carry the family torch to be a fourth generation geoscientist. Hope – you are my world and I cannot wait for our future together. No amount of words can express my gratitude for your constant celebration and support of my achievements, no matter how small or large they were. Dr. Bedle – I could not have asked for a better advisor. You pushed me to accomplish more than I could have ever imagined as an undergrad. Thank you for constant support. No other professor or teacher has made science. as fun and engaging as you.

Lastly, to all my friends I made at the University of Oklahoma, thank you all for making my time in Norman unforgettable. I was blessed with the best group of peers to go through the adventure of a graduate degree with.

Abstract

Silurian pinnacle reefs found within the Michigan Basin were prolific hydrocarbon producers in the mid-to-late twentieth century. During production, studies over these complex reservoirs were primarily focused on facies distributions and depositional environments interpreted from core and petrophysical log data. 2-D seismic was applied primarily for reef identification, and rarely incorporated in identifying facies. To date, only two studies using modern 3-D seismic data to characterize Silurian pinnacle reefs have been published (Toelle and Ganshin, 2018; Buist 2020). Toelle and Ganshin (2018) had poor well control, which significantly reduced the certainty of interpretations made. Buist (2020) utilized unsupervised Self-Organizing Maps for porosity and permeability correlation from seismic data in several reefs along the Southern Reef Trend. This study is the first to conduct a pre-stack seismic inversion over a Silurian pinnacle reef within the Michigan Basin, and both the pre-stack inversion volumes and post-stack seismic attributes are integrated with supervised and unsupervised machine learning techniques (Probability Neural Networks and Generative Topographic Maps) to characterize the reservoir properties of Ray Reef field along the Southern Reef Trend.

The workflow for this study begins with the well log data. A feasibility study is conducted to analyze relationships between elastic properties such as velocities and impedances, and reservoir properties such as porosity and lithology. Simultaneous pre-stack inversion is then conducted to provide P and S-impedance volumes, velocity cubes, and lambda-rho mu-rho volumes. Attributes are generated on the post-stack data as well, and input into the Generative Topographic Map (GTM) algorithm. The GTM is able to identify non-linear relationships between the attributes, and identifies relationships between lithology and seismic attributes. Pre-

stack inversion attributes are analyzed in traditional crossplots to classify zones of good, fair, and poor porosity. Probability Neural Networks (PNNs) are shown to excel at classifying the gas-water contact within the reservoir, in addition to delineating salt units from the encasing carbonate units.

The workflow described in this study identified a consistent relationship between lambda-rho and mu-rho attributes for porosity and possible fluid content within the Ray Reef gas storage reservoir in southeastern Michigan. Unsupervised machine learning techniques used also showed the ability to identify the reef core lithofacies from post-stack seismic data. These workflows have the potential to be applied on other pinnacle reef complexes within the Michigan Basin in addition to other carbonate reservoirs around the world.

Contents

Table of Figures

Chapter 1: Introduction

Motivation

The motivation for this study is to analyze and characterize geologic features within an active carbonate gas storage reservoir and extract quantitative measurements of reservoir properties from seismic data. Analyses are done using both pre-stack attributes derived from inversion and post-stack seismic attributes. The prolific Niagaran pinnacle reef reservoirs within the Michigan basin are now common targets for natural gas storage fields and carbon-dioxide sequestration. Both of these uses carry great importance for both the local and future populations. Natural gas storage helps ensure availability of energy during harsh winter temperatures, which can cause surges in demand. CO_2 sequestration studies of these pinnacle reefs could lead to widespread CO_2 sequestration within pinnacle reefs to combat rising concentrations, and possible EOR of remaining hydrocarbons. Understanding the spatial distribution of reservoir properties such as lithology and porosity is a key aspect of gas storage and can greatly enhance gas storage efficiency. Ray Reef field in Macomb County, Michigan, is one of the larger pinnacle reef storage reservoirs, with a total working capacity of 48 billion ft^3 of gas. It has been utilized for gas storage since 1966 after being a natural gas producing reservoir since 1959 (Gill, 1977). Carbonate lithologies are typically difficult to image in seismic data compared to siliciclastic lithologies due to their irregular pore geometry and crystalline matrix (Wang, 1997; Grammer, 2009; Trout, 2012). Seismic imaging is further complicated by the numerous salt units both above the reservoir interval, as well as encasing it (Jones and Davison, 2014). Seismic reflection data is also affected by diagenetic processes such as dissolution, cementation, and dolomitization. Carbonate lithologies are also difficult to distinguish using conventional well log analyses, due to the fact they have identical physical properties and differ in allochem or cement

composition (Grammar 2009). The above challenges impose a challenge on geoscientists efforts to map the spatial extent of lithofacies and reservoir properties away from well locations.

Ray Reef has been extensively drilled, with 84 wells within or nearby the pinnacle reef. Despite the dense well spacing commonly found in pinnacle reef reservoirs, little advancement was made on the understanding of the depositional framework of pinnacle reefs until recently (Mesolella, 1974; Gill 1977; Rine et al., 2017; Rine et al., 2020). To understand how seismic data and machine learning techniques can address these challenging imaging problems, several investigations incorporating modern depositional models are performed to analyze how each method can classify seismic facies in a heterogeneous gas storage reservoir within a mid-Silurian (Niagaran) pinnacle reef in the Michigan Basin. A high-resolution 3-D seismic survey that was acquired by Consumers Energy in 2019 includes conditioned pre-stack gathers and full-angle stack volumes over the Ray Reef. While the overall structure of the reef is well imaged, little information regarding the reservoir properties is revealed by the full-stack amplitude data. Well log data provides excellent vertical resolution, however the horizontal resolution is poor. Seismic data can supplement well log data in this sense as it has excellent horizontal resolution in comparison. A conventional lambda-mu-rho analysis was utilized to derive porosity from pre-stack inversion attributes. A suite of post-stack volume attributes influenced by previous studies (Buist et al., 2021) on nearby reefs is generated and Generative Topographic Maps (GTMs) are applied to identify multi-dimensional relationships between the seismic attributes for a data-driven classification of seismic facies. Seismic facies are identified via cross-plotting and constrained by available core data and detailed core profiles provided by Matt Rine to relate the seismic data to the geology, and provide a better understanding of the pinnacle reef reservoir.

Lastly supervised machine learning methods are tested for direct classification of seismic facies, and mapping of salt units around Ray Reef field.

Insights from this study can be incorporated in other Silurian pinnacle reefs in this region where seismic data is available, or future seismic acquisition to enhance reservoir management. As many of the reefs are vintage reservoirs, they typically lack complete petrophysical datasets. For example, the majority of the log suites available for this study included gamma ray and neutron count, with occasional neutron porosity and density logs available. By incorporating the proposed seismic data analyses into well planning and reservoir management, uncertainties associated with encountering locations with undesirable storage and/or flow properties can be reduced compared to just using well data. In order to effectively utilize the data generated in this study, understanding the changes of depositional environments and associated facies, such as the reefal frame building organisms observed are important. Events such as relative sea level and salinity fluctuations, wind direction, and oxygen levels can promote or halt reef growth, which can impact deposition of potential reservoir quality rocks (Trout, 2012). As the reservoir is dolomitized, the process in which dolomitization is also important to understand, as certain reservoir zones can have enhanced porosity from dolomitization while others can have porosity reduced. In the case of the Ray reef, the entire reef complex has been overprinted by secondary dolomitization. Workflows demonstrated herein display ways to overcome the limitations of incomplete petrophysical log suites to assign quantitative measurements of reservoir properties from seismic facies and also discuss the possible associated pitfalls.

Chapter 2: Seismic characterization of the Ray pinnacle reef reservoir

Geologic Setting: Michigan Basin, USA

The Michigan Basin is an intracratonic basin which exhibits unusual circular symmetry and is relatively undeformed. The basin covers an area of 316,000 km^2 (Catacosinos et al., 1991). It is bounded in the East by the Findlay-Algonquin Arch, the south by the Kankakee Arch, to the West by the Wisconsin Arch, and to the North by the Canadian Shield (Figure 2.1).

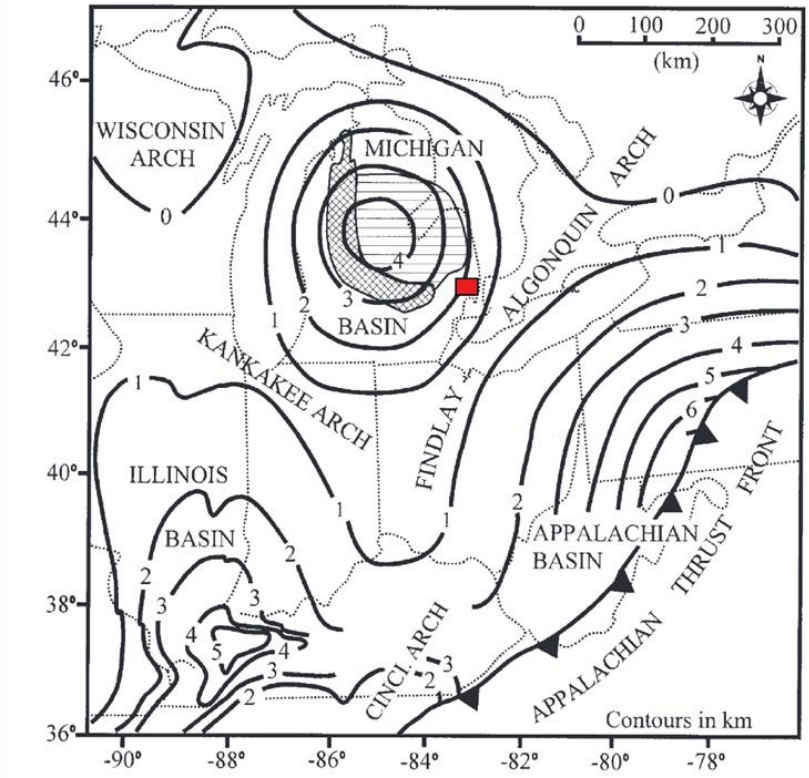

Figure 2.1: Regional map displaying the total thickness of Phanerozoic sedimentary rocks in the Michigan Basin. The study area is represented by the red box. Modified after Howell and Pluijm (1999).

The Michigan Basin was likely initiated as a northern continuation of the Illinois Basin area that formed in response to Cambrian extension (Sleep et al., 1980). Evolution of the basin from the Cambrian through the Ordovician can be divided into four episodes (Howell and Pluijm, 1990; Howell and Pluijm 1999):

a) Early extension-related subsidence (late Cambrian-early Ordovician)

b) Initial basin-centered subsidence (mid Ordovician)

c) Regional eastward tilting toward the Appalachian Basin (late Ordovician-early Silurian)

d) Renewed basin-centered subsidence (early Silurian-end Silurian)

Throughout the Silurian, basin-centered subsidence was the primary control on sedimentation (Zheng, 1999, Haynie, 2009). During the Niagaran (mid-late Silurian), the Michigan basin was in the southern equator, around 20-25° in a tropical environment which promoted reef growth (Figure 2.2) (Scotese, 2002, Rine et al., 2017). Basin centered subsidence directly affected reef growth, as Niagaran pinnacle reefs found on the upper shelf are characterized by a large lateral extent and lower vertical extents. Pinnacle reefs on the lower shelf are typically taller and have a lesser lateral extent (Gill, 1977, Sears and Lucia, 1979). Reef development was concentrated along two parallel lineaments along the northern and southern rims of the Michigan Basin trending northeast-southwest. These trends are referred to as the

northern and southern reef trends respectively. Carbonate deposition is attributed to the

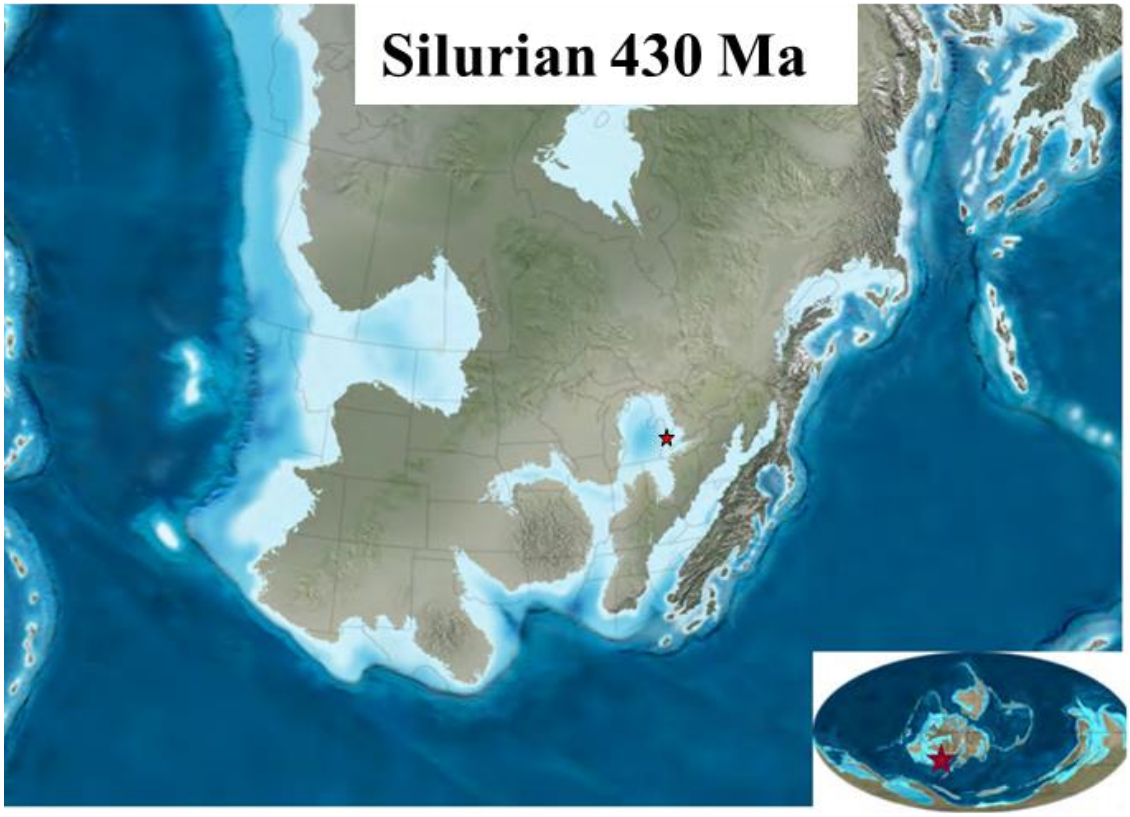

Figure 2.2: Paleogeographic map of the Silurian approximately 430 Ma. Ray Reef is located at the red star. (Modified after Scotese, 2002).

beginning of a wide spread transgression of the continental platform (Briggs, 1978, Rine 2015). By the late Niagaran, restriction and isolation of the basin from open seas resulted in a cessation of reef growth and marked a transition to an arid, restricted marine depositional environment (Briggs, 1978). This resulted in the deposition of the Salina group, which is primarily comprised of evaporites with some restricted carbonate successions. The Salina Group is capped by relatively thick carbonate units deposited in a restricted marine environment, which represents the final stage in carbonate deposition. Following deposition of the lower Salina group, the Michigan Basin was isolated from surrounding seas which resulted in continuous deposition of thick evaporite units.

Southern Reef Trend Stratigraphy

The litho- and chronostratigraphy of reefs along the southern reef trend is well

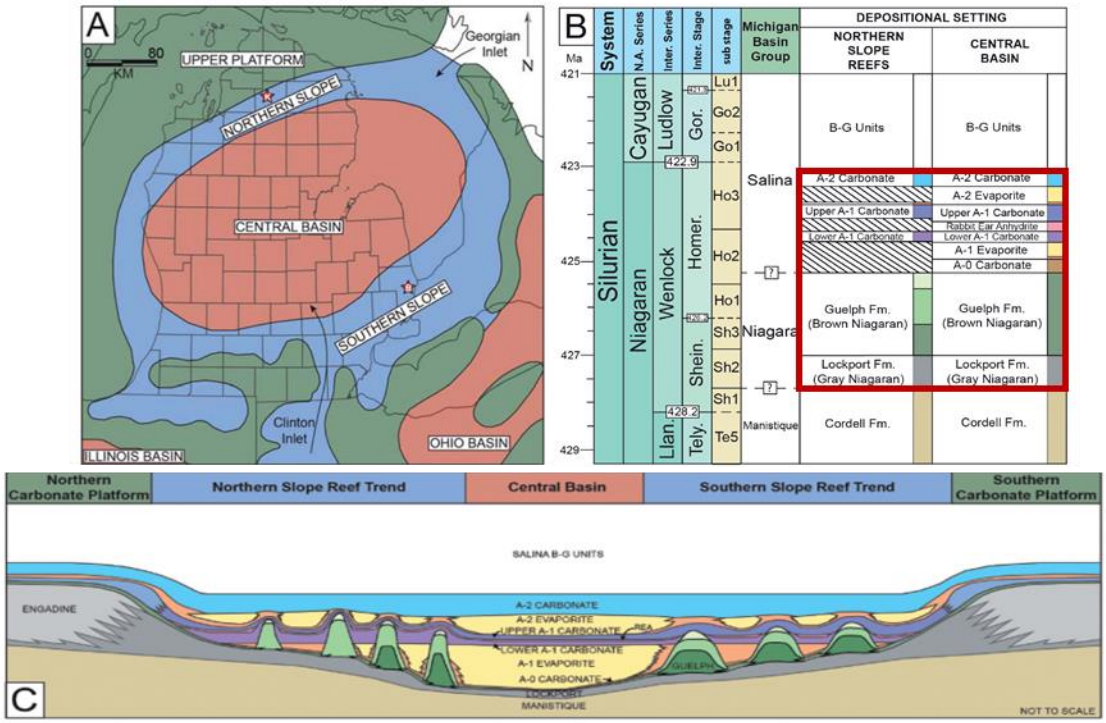

Figure 2.3: Overview of the Michigan Basin modified after Rine et al. (2017). A- Overview of the general depositional environments of the Niagaran. B- Chronostratigraphic column with the studied interval outlined in red. C – Representative cross section across the Michigan Basin illustrating the two reef trends within the basin.

established (Figure 2.3). The upper Silurian deposits in the Michigan Basin are split into three groups: The Manistique, Niagara, and Salina Groups (Catacosinos et al., 2001; Rine et al., 2020). For this study, the lower Manistique Group is not investigated. The Niagara Group represents a bioclastic ramp facies succession and is divided into several formations. The Niagara Group thins basinward, from approximately 300 feet on the shelf to less than 90 feet in the central portion of the basin (Mesolella et al., 1974; Armstrong and Carter, 2010; Rine et al., 2020). The lowermost formation is the Lockport Formation (informally called the "Gray Niagaran"), which

is described as a gray micritic carbonate (Rine et al., 2017). Pinnacle reefs overly the Lockport Formation and occur within the Guelph Formation (also referred to as the "Brown Niagaran"). On the slope, the Guelph Formation is typically less than 30 feet thick, and is thickest where pinnacle reefs developed to thicknesses of 300-500 feet. Within the reefs, a variety of deep-water and shallow marine facies are present (Mesolella et al., 1974; Huh et al., 1977; Sears and Lucia, 1979; Wold, 2008; Haynie, 2009; Trout 2012; Rine 2015). Pinnacle reefs of the Guelph Formation are encased and overlain by the restricted carbonates and evaporites of the Salina Group (Huh et al., 1977; Sears and Lucia, 1979; Rine et al., 2017). The Salina Group is split into multiple carbonate and evaporite formations. The lowermost, the A-0 Carbonate, is typically composed of thin carbonate and anhydrite (Leibold, 1992). The A-1 Evaporite overlies the A-0 Carbonate, and is composed of halite and anhydrite. The A-1 Evaporite onlaps onto the Pinnacle reefs within the Guelph Formation (Wold 2008, Haynie, 2009). The A-1 Carbonate (formally the Ruff Formation) in our study area is dolomitized and overlies the pinnacle reefs (Wold, 2008; Haynie 2009; Trout 2012). A variety of facies are present within the A-1 Carbonate. Atop pinnacle reefs, it is characterized as a peritidal deposit, likely within a tidal flat environment as stromatolite boundstones and peloidal grain to mudstones are present in core. In the inter-reef region, the A-1 Carbonate is an organic-rich, laminated carbonate mudstone (Sears and Lucia, 1979; Rine 2015; Rine et al., 2017). Recent studies have subdivided the A-1 Carbonate into the Lower A-1 Carbonate, Rabbit Ears anhydrite, and the Upper A-1 Carbonate (Haynie 2009, Rine et al., 2017). The A-2 Evaporite overlies the Upper A-1 Carbonate, and is typically composed of halite deposits. Within the Ray Reef study area, it is represented by a 20 to 50 ft thick anhydrite deposit and acts as the overlying seal for the reservoir. The A-2 Carbonate is the youngest

formation in the Salina Group studied, and represents the final period of carbonate deposition within a restricted marine environment (Rine et al., 2017; Rine et al., 2020).

Pinnacle Reef Development

Numerous models have been proposed to explain the development of Niagaran pinnacle reefs (Jordy, 1969, Mesolella et al., 1974; Gill, 1977; Huh et al., 1977; Sears and Lucia 1979; Rine et al., 2017). While most of the early proposed models varied slightly on relative timing of deposition of Guelph and Salina Group formations, all of the models presented the pinnacle reefs as having tall and symmetric geometries. The classical models also presented pinnacle reefs as

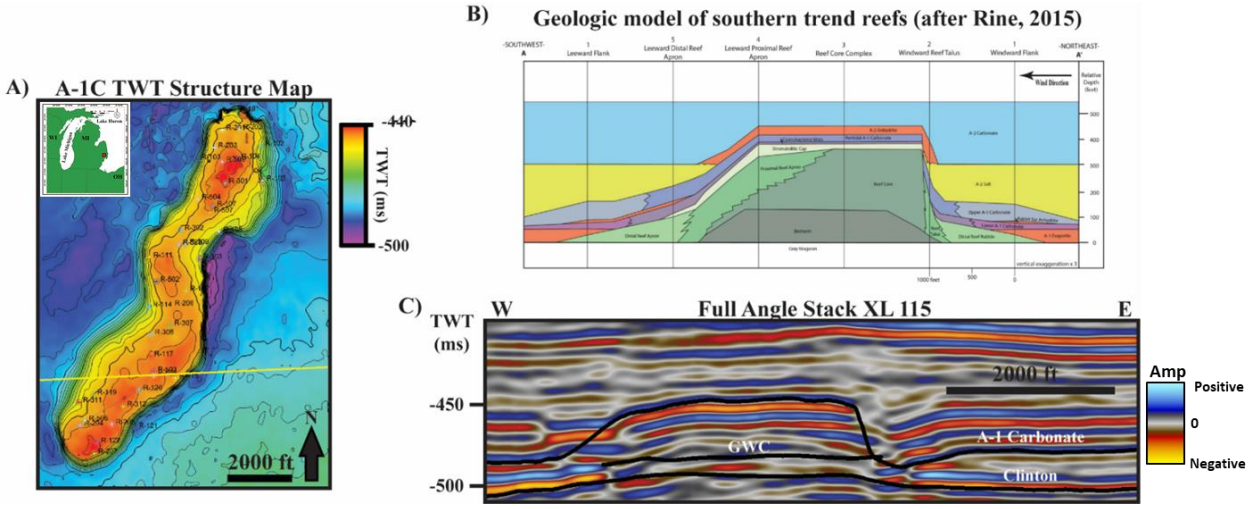

Figure 2.4: A- Two way time (TWT) structure map of the top A-1 Carbonate within Ray Reef. B- Geologic model of Niagaran pinnacle reefs proposed by Rine, 2017. C- XL 115 of the 3-D post stack seismic amplitude volume. The seismic data accurately matches the geometries of the proposed core-based geologic model.

having a patchy, unpredictable distribution of lithofacies. Rine (2017, 2020) proposed a new depositional model which utilized multiple fields with numerous cored wells available. In this model, pinnacle reefs are identified as having a predictable distribution of lithofacies, in addition to being structurally asymmetrical (Figure 2.4). Paleo-winds oriented from the modern-day east to northeast resulted in southern trend reefs to have a steeply dipping (~60°) windward flank with a gently dipping (~15-20°) leeward flank (Figure 2.4b). Reef development occurred in

several distinct stages (Figure 5). First, the bioherm initiated growth upon the Gray Niagaran in water depths below the storm-wave-base (SWB). Growth of the bioherm resulted in

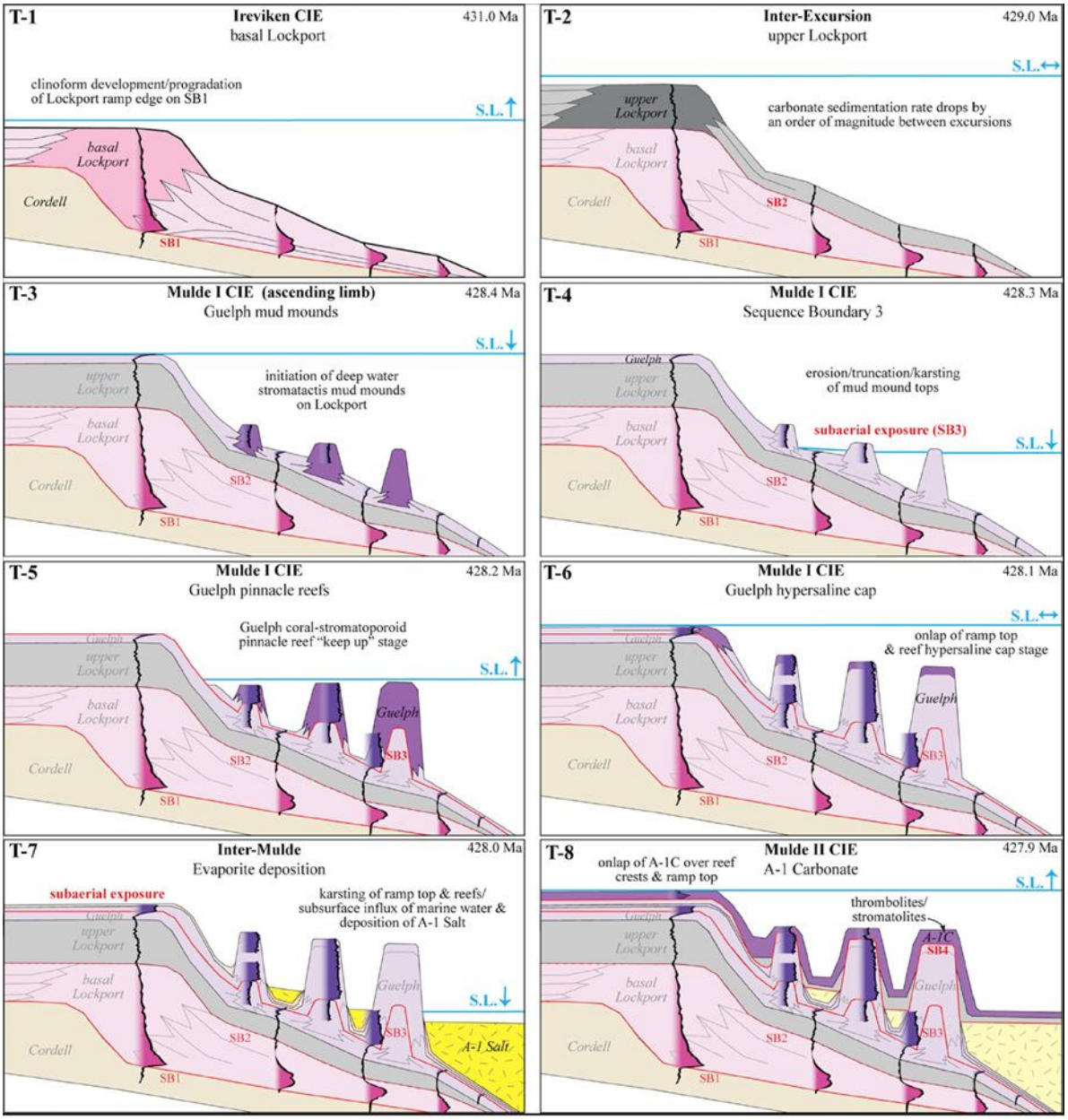

Figure 2.5: Illustration of the key depositional sequences that influenced Niagaran pinnacle reef growth in the Michigan Basin proposed by Rine et al (2021).

encountering higher-energy environments, and a gradual increase of corals and stromatoporoids is observed near the cap of the bioherm. The bioherm and reef core are separated by a small unconformity that is likely an exposure surface (Wold 2008; Rine et al., 2020). Following a rise

in relative sea level (RSL), reef growth was initiated. Rapid reef growth due to keeping up with RSL rises resulted in the formation of the reef apron facies. Typically, the leeward apron has a larger aerial extent than the windward and is composed of finer grained deposits. Windward apron facies are conglomeritic and do not span far from the reef core. The next stage of reef development is the deposition of a stromatolitic cap, which was deposited in a high-energy intertidal deposit. A drop in RSL resulted in the full to partial exposure of the reef complex, and deposition of the A-0 Carbonate begins. A continued decrease in RSL resulted in hyper-saline oceanic conditions in addition to karsting and initial dolomitization of the reefs (Zheng, 1999). The A-1 Salt was deposited, which gradually pinches out toward the southern reef trend. A brief, relatively small rise in RSL deposited the lower A-1 Carbonate on the flanks of the reefs, and high-order fluctuations deposited the Rabbit Ears Anhydrite on the flanks of reef complexes. Sea level rose above the reef crest following REA deposition, and the carbonate factory was re-established depositing the Upper A-1 Carbonate. On the reef crest, this is represented by a series of cyclical peritidal deposits marked by upward shallowing deposits with thin discontinuities. RSL fell again following Upper A-1 Carbonate deposition, and the A-2 Evaporite was deposited. This unit unconformably overlies the Upper A-1 Carbonate, and is composed of anhydrite on the crest and halite on the flanks. Finally, as basin waters freshened, the A-2 carbonate was deposited. This marked the final phase of carbonate deposition within the study interval. The A-2 Carbonate filled in depressions of the reef and marked the end of the topographic influence of pinnacle reefs.

While the stratigraphy of the reefs is understood, the relationship of porosity and permeability to depositional facies is uncertain. By incorporating Rine et al's facies model for pinnacle reef architecture in conjunction with previous petrophysical models over Ray Reef

(Wold 2008; Haynie 2009) with modern seismic data, this study aims to investigate how seismic data can image the distribution of these key reservoir properties.

Ray Reef Field, Michigan Basin

Ray Reef 3-D Seismic Survey

One seismic survey is used in this study: Ray3D (Figure 2.4a). This survey was acquired and processed in late 2019. Ray3D was contracted by Consumers Energy, the operator of the gas storage field, and processed by Sterling Geophysical. Ray3D is 9.4mi^2, has an inline and crossline spacing of 110ft, station spacing of 110ft (55ft bins), a 2 second record length, and 1 millisecond sample rate. Three volumes were initially available: pre-stack time migrated (PSTM) full angle stack, a 0-10 degree angle stack, and a 20-30 degree angle stack. In October 2020, pre-stack offset gathers for the survey were also made available. The gathers have been processed by geophysicists at Sterling Geophysical using a standard amplitude-preserving processing workflow and are of good quality. The PSTM full angle stack accurately captures the overall structure of the reef, however it images the flanks of the reef poorly likely due to their steep dips (Figure 2.4c). Using a smooth velocity model from the DT log in well 24224 located off the reef and R-117 located within the southern part of the reef, angles up to 30 degrees are available at the time interval of the reef. Seismic resolution is estimated at 50 ft at the reservoir interval. Ray3D has SEG positive polarity, where an increase in acoustic impedance is represented by a peak in the seismic amplitude data. It is important to note that at the time of seismic acquisition, Ray Reef was at near full storage capacity of 64.5 bcfg out of a total storage capacity of 65.4 bcfg.

Ray Reef Well Dataset

There are 84 wells within Ray3D. Formation tops and core descriptions were interpreted and provided by Matthew Rine from Consumer's Energy. Fifteen of these wells are cored with core measured porosity and permeability (Figure 2.6). Seven cored wells have core facies

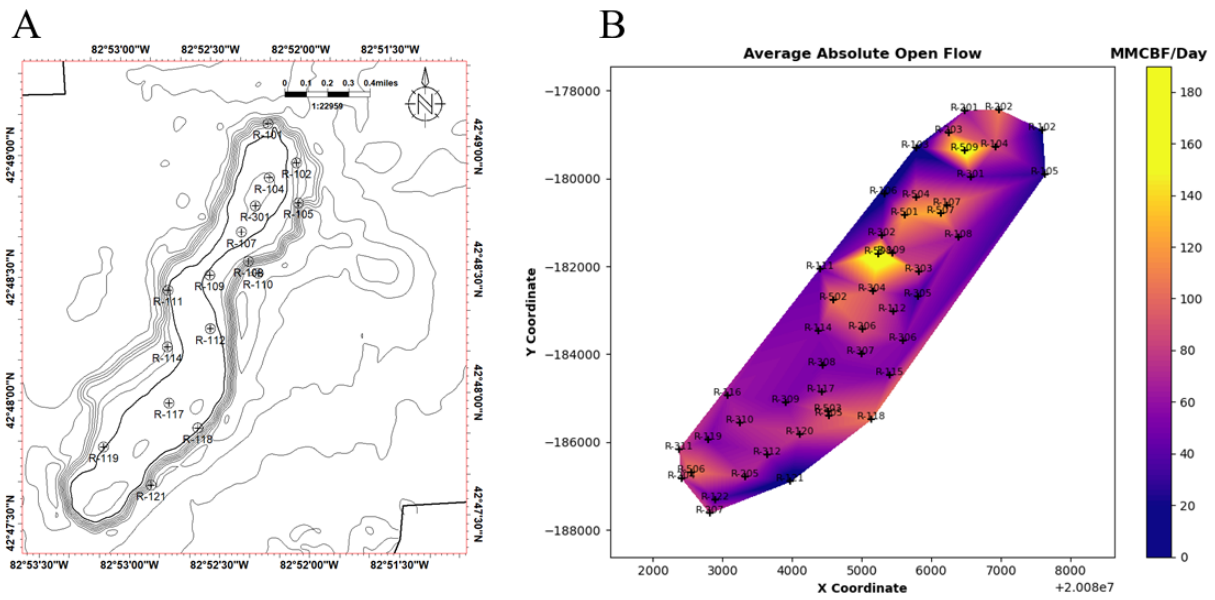

Figure 2.6: A- Map of cored well locations within the Ray Reef field. TWT contours are shown in 5 ms intervals. B- Average absolute open flow (AAOF) map of 40 active storage wells.

descriptions done by professional geologist Matthew Rine in addition to water and oil saturation measurements. Due to the legacy nature of Ray Reef Field, it has a relatively poor suite of petrophysical logs available in non-cored wells. Many of the wells provide a combination of either Gamma Ray, Neutron, and/or Resistivity logs. Neutron logs were converted from neutron count to neutron porosity logs following the methods of Shier (1991) and Haynie (2009). 7 wells have sonic logs and 6 wells have density logs, however just one well has both sonic and density logs and is located off the reef complex (Well 24224). This is important to note as sonic and density logs are crucial for calculating time-to-depth relationships to integrate well data that is in

depth with the seismic data, which is in the time domain. Additionally, Average Absolute Open Flow (AAOF) for 40 operating storage wells was provided (Figure 2.6b). AAOF is a calculation of what the well would flow to atmosphere if there were no surface restrictions. This provides a normalized value of flow rates which allows for comparison of well performance independent of the back pressure on the well at surface. The units for AAOF are Million Cubic Feet per Day (MMCFD).

Gardner's relationship between velocity and density is applied to predict the respective missing logs in wells with either sonic or density logs present (Gardner, 1974). Following density and sonic log estimation, shear velocity logs were generated using the workflow proposed by Xu et al. (2007). The authors propose a model whereby limestones contain a variety of pore types which can be modeled by different aspect ratio inclusions. As the reservoir is completely dolomitized, mineralogical estimates for dolomite density were used rather than limestone. A density of 2.87 g/cm^3 were used for dolomite within the reservoir with an aspect ratio of 0.20 for the macroporosity and 0.05 for the microporosity. The calculated Vp/Vs logs do not provide any values below the theoretical limit of 1.41, so the estimated logs are deemed satisfactory given the available data. Once well log estimation is completed, the wells with sonic and density logs were tied to the seismic data to construct a time-to-depth relationship.

Methods

The motivation of this study is to analyze the feasibility of identifying seismic facies utilizing interpreter knowledge aided by machine learning techniques and relate the seismic facies to lithology and/or variations in porosity. A seismic facies is defined as a geological unit which is distinct from adjacent and surrounding units in its seismic characteristics (Roksandic,

1978). While seismic amplitude data allows for mapping of formation tops away from well locations and observing general structure, post-stack amplitude data alone provides little quantitative information regarding changes in lithology, depositional environment, or reservoir quality. The following sections will review a variety of methods tested in this study to transform post-stack seismic data to measurements of different characteristics, and machine learning workflows used to identify non-linear relationships between these data.

Post Stack Seismic Attributes

A seismic attribute, defined by Chopra and Marfurt, (2005) is a quantitative measure of a seismic characteristic of interest. The goal of seismic exploration is to identify and characterize the static and dynamic characteristics of subsurface reservoirs. A good seismic attribute is either directly sensitive to the desired geologic feature or reservoir property of interest or gives insight to the depositional environment and/or structure, thereby allowing the interpreter to infer some feature or properties of interest. Instantaneous attributes provide better visualization of bedding continuity and lithology contrasts. Geometric attributes highlight discontinuities such as faults, fractures, and folds (Chopra and Marfurt, 2005).

Previous studies over Niagaran reefs investigating unsupervised machine learning techniques applied to post-stack seismic data have identified that frequency-based and instantaneous attributes have the potential to differentiate high and low porosity and permeability zones from volume attributes (Toelle, 2018; Buist, 2020). For this study, a similar suite of volume attributes is generated on each volume. This included: Instantaneous frequency, cosine of instantaneous phase, and iso-frequency volumes output from spectral decomposition. Instantaneous phase is defined as the arc tangent of the ratio of the imaginary and real parts of the seismic trace (Taner, 1978). It is independent of amplitude and is related to the propagation

of the seismic wave front and can be applied to analyze stratigraphic continuity and configurations (Barnes, 2016). As instantaneous phase is a cyclic attribute, the cosine of the instantaneous phase is chosen to avoid the cyclic values as the GTM algorithm will interpret the discontinuity in the phase at 90° and -90° as different values, when in reality they are zero crossings. With cosine of instantons phase, zero crossings are represented by values of zero and correctly interpreted by the algorithm. Instantaneous frequency is the time derivative of instantaneous phase. Low instantaneous frequency values have been shown to correlate to high porosity zones within Niagaran reefs along the northern reef trend (Toelle, 2018). This relationship was interpreted to be caused by attenuation of the seismic wave front caused by the increase in pore space. Three iso-frequency cubes from spectral decomposition were also used as input using a continuous wavelet transform (CWT). Nejad et al. (2009) applied spectral decomposition utilizing the CWT method to image reef structure and also delineated regions of high and low porosity within the reef. Another study of frequency attributes in carbonates related low frequency shadows observed in frequency volumes from CWT spectral decomposition to hydrocarbon accumulations (Saadatinejad et al., 2012). For this study, 24, 53, and 87 Hz frequency components were chosen based on their strong response observed in the spectral domain, and these frequencies highlighted internal variations within the reef.

Pre Stack Inversion

All AVO studies are based on the plane wave Zoeppritzs equations, which model a plane wave in terms of P and S wave velocity and density. However, due to the complexities of Zoeppritzs equations, approximations are commonly used. Pre-stack simultaneous inversion implemented by the Hampson-Russell software utilizes the Fatti et al. (1994) extension of the

Aki-Richards (1980) approximation of Zoeppritzs equations (Hampson and Russell, 2005). Fatti et al. (1994) reformulated the Aki-Richards formula so that the reflectivity as a function of angle is represented by the P-impedance and S-impedance rather than velocity and density. Integrating the reflectivity component in Fatti's equation provides the P-wave and S-wave impedances from pre-stack seismic gathers. The inversion workflow used also provides P-wave and S-wave velocity attribute cubes. The resulting residual error cubes were also saved as volume attributes. These provide a measure of the difference between the seismic full spectrum inversion attributes and the low-frequency background model. Due to the low maximum angle range (angles < 30°), a stable density cube was not able to be produced from the inversion. The simultaneous inversion method used is a deterministic method – which means the inversion result will provide one single solution that minimizes the error between the initial model and the reconstructed synthetic seismic output from the inversion. This method is advantageous for this dataset as the limited well control and strong understanding of the geology allows the interpreter to impose constraints on the seismic inversions to honor the structure and stratigraphic relationships within Ray Reef. The goal of the pre-stack inversion is to remove the wavelet from the seismic data and to transition from an interface property (seismic amplitude) to a layer property (impedance) which allows for more direct geologic interpretations (Maurya and Sarkar, 2016).

The low frequency model (LFM) constructed in this study utilized 3 wells: Well 24224, located off the reef, Wells R-117 and R-207 which are both located within the reef. Well 24224 was selected as it provides good control of lithologies encountered off the reef, and has both sonic and density logs. Well R-117 has a measured sonic log and estimated density log, while Well R-207 has a measured density log and estimated sonic log. Additionally, Well R-207 provides accurate density values for the capping A-2 Anhydrite. All wells have a calculated S-

wave velocity log. Four interpreted horizons were used as input: The A-2 Carbonate, A-2 Salt, A-1 Carbonate, and the Clinton formation horizons. The model honors the stratigraphic relationships of the reef complex. The A-2 Salt onlaps and is truncated by the A-1 Carbonate horizon, and a follow-top layering solution was used for the A-1 Carbonate zone. The LFM is a crucial part of the inversion process, as seismic amplitude data is band-limited and is missing low-frequency information (Chopra and Castagna, 2014). The well log data is smoothed with a 30 sample median filter within each defined zone and interpolated between well locations using an inverse-distance weighting algorithm.

Angle Versus Offset (AVO) Attribute Analyses

Angle versus offset or Angle Versus Angle (AVO/AVA) analysis exploits and extracts variations between P-wave and S-wave velocities to identify lithological and fluid properties (Castagna 1993; Goodway et al, 1997; Chopra and Castagna, 2014). AVO has been a common workflow to identify potential hydrocarbon exploration prospects and to give insight to lithology, porosity, and possible fluid content from seismic data (Ostrander 1982; Goodway et al., 1997; Chopra and Costagna 2014; Sams et al., 2017). Challenges do arise with carbonate reservoirs and AVO methods, as their pore structures are typically heterogeneous, especially in dolomite reservoirs. Porosity types can vary from intercrystalline, vuggy, moldic, channels and fracture porosity (Wang 1997; Trout 2012). In Ray Reef, analyses of core from a variety of depositional environments (i.e. windward talus, reef crest, leeward apron) suggest secondary dissolution can completely replace, fill, or enhance existing porosity (Trout 2012). In addition to complicated pore structures, the reduction in P wave velocity (and Vp/Vs) associated with the presence of gas observed in siliciclastic rocks is typically not as dramatic in carbonates due to carbonates being

less compressible than unconsolidated sandstones (Chopra and Castagna, 2014). Despite these shortcomings, AVO workflows that were originally developed for unconsolidated sandstone reservoirs have been successfully applied to numerous carbonate reservoirs (Harvey 1993; Li et al., 2003; Mahmoud et al., 2009; Chopra and Castagna 2014). Using the Zp and Zs inversion attributes, lambda-rho and mu-rho (LMR) volumes were calculated (Russell, 2003). Lambda-rho is defined as: $\lambda\rho = Z_P^2 - cZ_S^2$ and mu-rho is: $\mu\rho = Z_S^2$. Lambda (λ) and mu (μ) are the Lamé's constants of compressibility and rigidity respectively (Goodway et al., 1997, Goodway 2006). It is important to note that LMR attributes do not contain any information that are inherently new in regards to the Zp and Zs inversion attributes, as they represent a transformation of data present in the P and S impedance volumes. The squaring of the impedances does allow for larger separation of data points, and previous studies have related variations present within LMR space to lithology, porosity, and pore fluids. Furthermore, as the local structure is well known and the reservoir is completely dolomitized, these templates can guide classification of seismic facies which correspond to favorable reservoir zones.

Generative Topographic Mapping (GTM)

The Generative Topographic Mapping algorithm (Bishop et al., 1998) is a non-linear dimensional reduction technique, allowing interpreters to analyze multi-dimensional relationships between multiple seismic attributes in a two dimensional latent space. It was formulated as a probabilistic extension of the popular self-organizing map (SOM) algorithm that is commonly applied to seismic data. GTM addresses some shortfalls of the SOM algorithm, such as the inability to initialize framework parameters, and no measure of convergence of the algorithm. Roy (2013) provides a comprehensive analysis and review of the mathematical implementation of GTM to seismic data. In summary, GTM represents the distribution of multi-

dimensional data vectors by a 2-D deformed manifold that iteratively adjusts to best fit the data in data space (Roy, 2013). A set of non-linear basis functions is used to map points to the dimensional latent space into the manifold within the data space. Data vectors are modelled by a suite of Gaussian PDFs centralized on the mapped grid points on the manifold, which is used to define the space in which the data vector lies (Figure 2.7). This initial portion is referred to as a constrained Gaussian mixture, as the Gaussian centers are constrained by the grid points within

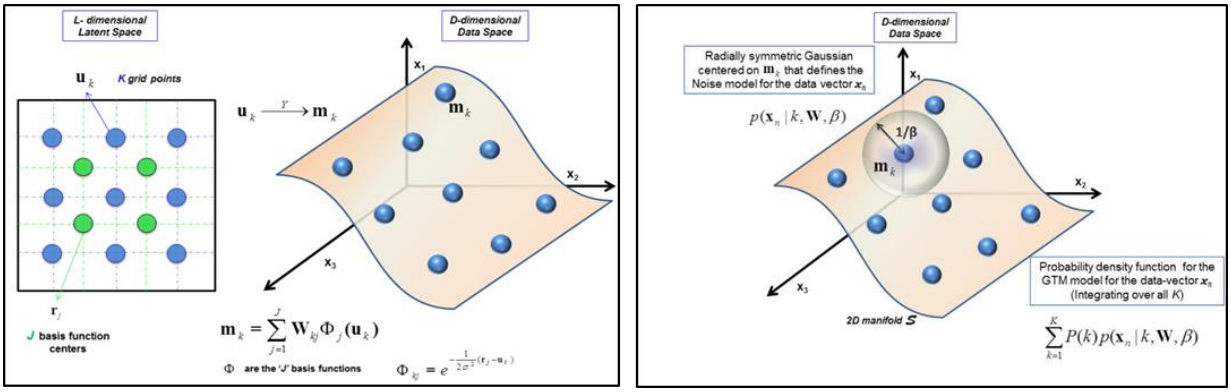

Figure 2.7: Illustration from Roy (2013) which shows the transformation of grid points from latent space to data space, and the Gaussian centers within the D-dimensional data space

the latent space. Through each iteration, components of the mixture model are moved towards the data vector that represents it best. An expectation maximization algorithm is used to update the mapping parameters for each iteration. The probability of a data vector being represented by the 2D manifold can then be calculated and used for visualization.

The individual post-stack attribute volumes were used as input for the unsupervised GTM algorithm. The algorithm analyzes the data points in an n-dimensional (in this study, n=5 as 5 attribute volumes were used) data space. Once a best fit is reached, the mean responsibility of a data point residing within this 2-D manifold is calculated, and the X and Y coordinates for each voxel is output to a respective SEG-Y cube. These X and Y coordinate cubes can then be cross plotted using either a 2-D color bar or crossplotting software. The data points which correspond

to the investigation box are highlighted in the cross-section and user-defined polygons are then drawn around the data points while also honoring the natural clusters of the GTM output. Polygons are iteratively adjusted using in-context interpretation to appropriately correlate to other well locations. All data points within a polygon are assigned a single discrete value, or class, and a discretized SEG-Y volume is output by the software once a satisfactory classification is achieved. This workflow allows the interpreter to impose their geologic knowledge as a form of "supervision" on the unsupervised GTM algorithm. As only the reef complex itself is being target for gas storage, the GTM algorithm was limited spatially to only the reef complex and vertically between the top of the A-1 Carbonate and the top of the underlying Clinton Formation.

Seismic Facies Classification

To identify seismic facies, crossplots of seismic attributes were used. Initially, crossplots were introduced seismic data to visually analyze the relationship between two to three variables (White, 1991). With the introduction of AVO analyses, crossplotting became a common tool to identify AVO anomalies (Hilterman and Verm, 1994). With the recent emphasis on quantitative interpretation (Chopra and Marfurt, 2006; Chopra and Costanga, 2014), crossplotting of elastic properties derived from seismic inversion has been shown as a powerful tool for delineating high-quality reservoir zones (Bellman, 2018). To relate the unsupervised classification and inversion attributes to the geology, the data corresponding to cored wells is analyzed first. Using a nested cross-plotting software, investigation boxes are drawn at cored well locations within the pinnacle reef reservoir. The data points which correspond to the investigation box are highlighted in the cross-section and user-defined polygons are then drawn around the data points. Polygons are then iteratively adjusted using in-context interpretation to appropriately correlate to other well locations. All data points within a polygon are assigned a single discrete value, or class, and

a discretized SEG-Y volume is output by the software once a satisfactory classification is achieved. This workflow allows the interpreter to use a data-driven classification while honoring the clusters within unsupervised GTM algorithm, and constrain classifications of the inversion attributes.

Hydraulic Flow Units (HFU)

Hydraulic flow unit classification is carried out on the basis of Flow Zone Indicator values. While graphical clustering from a log-log plot is the simplest method of HFU classification, it is not sufficient to determine cutoff values between HFU's, especially in a dataset with numerous permeability and porosity logs such as Ray Reef (Dezfoolian et al., 2013). A hierarchical clustering analysis was employed on the log FZI values to overcome the limitations of graphical clustering (Pedregosa et al., 2011). The Agglomerative clustering method used is initialized by setting the number of flow units equal to the number of samples, and iteratively merging samples with similar log FZI values into distinct clusters. Several methods of linkage criteria for cluster merging are available, and the Ward method was selected as this method minimizes the sum of squared differences within all clusters (Pedregosa et al., 2011). As agglomerative clustering requires the number of clusters as a known input, similar to K-Means, the sum squared distance was calculated for a variety of number of HFU's. The results of this test show that any increase in the number of HFU's past four does not significantly reduce the reduction in flow unit estimation error (Figure 2.21). A histogram plot is used as conformation of this, as the FZI values typically exhibit a superposition of log-normal distributions for each respective distinct flow unit (Amaefule et al., 1993). The histogram confirms that four HFU's will make a good approximation for classification (Figure 2.21). The resulting classification of HFU's correlate well in the log-log plot of RQI vs ϕ_z (Figure 2.21). HFU 2 consists of the best performing reservoir zones, with high porosity and permeability values. HFU 0 and 3 consist of average to

below average reservoir zones, and HFU 1 is the worst performing reservoir zone with the lowest porosity and permeability values.

Probabilistic Neural Networks (PNN)

Probabilistic Neural Networks (PNNs) are feed forward neural networks and are a form of supervised classification first proposed by Specht (1990), which gives an example architecture for the framework of a PNN. PNNs determine decision boundaries for classification utilizing probability density functions (PDFs) using Parzen windows and Bayes criteria (Specht 1990; Hajmeer and Basheer, 2002, Lubo-Robles 2020). Bayes criteria is a strategy in which classified patterns minimize the expected risk (Mood & Graybill, 1962; Specht 1990). As the probability densities of the patterns of the categories desired to be separated are unknown and only the training data are available, the PDFs are estimated within each training sample. For a given set of training data (in this case seismic attributes) **a**, the average estimated density function g(**a**) is: $g(\boldsymbol{a}) = \frac{\mathbf{1}}{\boldsymbol{N}}\sum_{\boldsymbol{N=1}}^{\boldsymbol{N}} \boldsymbol{e}^{-\sum_{\boldsymbol{m=1}}^{\boldsymbol{M}}\frac{(\boldsymbol{b_m}-\boldsymbol{a_{nm}})^{\mathbf{2}}}{\mathbf{2}\boldsymbol{\sigma}^{\mathbf{2}}}}$, where M is the number of training attributes, N is the number of training samples, **b** are the validation attributes that we aim to classify, and σ is a smoothing parameter. The PNN begins by computing the distance between validation and training attributes, which is then input into the Gaussian activation function (Masters 1995; Lubo-Robles 2020). The average estimated density function is calculated in the summation layer, and then the output layer is where the PNN classifies the unknown sample based on which estimated density function is largest. PNNs also provide confidence of the resulting classification after Masters, 1995: $P[A|B] = \frac{g_A(B)}{\sum_j g_j(B)}$ where P is the probability of an observation B be the product of class A, $g_A(\mathbf{a})$ is the estimated density function for class A, and J represents the number of classes. The

PNN as described above only requires optimization of one parameter, the smoothing parameter σ. This is optimized following Lubo-Robles' (2020) workflow where the minimum error E is given by: $E = \sum_{r=1}^{R} \frac{e(r)}{R}$, where R is the number of validation samples, and e is equal to one if the validation sample was misclassified or zero if the sample was correctly classified. A range of values for σ is tested starting at 0.1 to 5 in increments of 0.5. The error E is computed for each iteration for each training sample and for each possible attribute combination. Following testing, the attribute combination and corresponding σ value is selected for classification salt and carbonate facies from seismic data.

Exploratory Data Analysis

Prior to conducting the pre-stack inversion, the petrophysical well logs must first be analyzed to determine if the inversion will provide meaningful data. The petrophysical analyses are initialized by tying the wells to the seismic data (Figure 2.8). A statistical wavelet is extracted over a 75 ms window from the post-stack seismic data. The wavelet is then convolved with a computed P-impedance well log to create a synthetic seismic trace. The synthetic seismic trace is shifted to match well tops with prominent reflectors (Figure 2.8). Once a time-to-depth relationship is created at well locations with sonic or density logs, a series of well log cross-plots are created to understand the relationships between rock physics parameters measured in the seismic amplitude data. In general, the seismic amplitude response of a given subsurface interface is dependent on contrasts in density, P-wave and S-wave velocities (Chopra & Castagna, 2014). These factors are influenced by geological variations within each layer, such as lithology, mineralogy, porosity, stress, pressure, and pore fluid content (Castagna et al., 1993).

As no laboratory measurements are available of elastic rock physics parameters and no

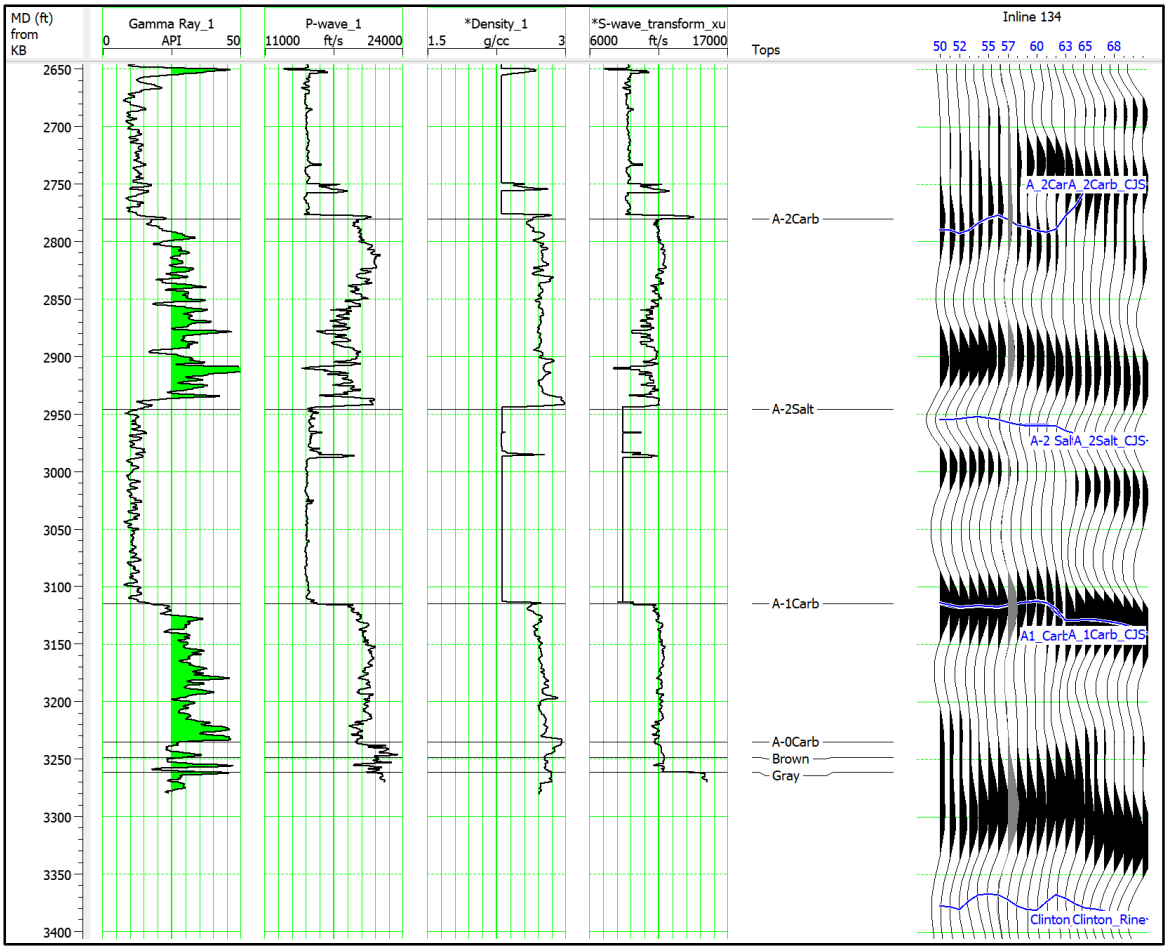

Figure 2.8: Well 24224 log suite and well-to-seismic tie. The S-wave was predicted using Xu et al. 2007 method. A correlation coefficient of 0.8 was achieved for the well tie. Note the A-0 Carbonate, Brown, and Gray formations are sub-seismic resolution off the reef.

wells that penetrate the reef reservoir have a complete log suite, variations in porosity, Zp, Zs, and Vp with respect to lithology are utilized to understand what the seismic inversion may reveal. The goal of these cross-plots is to see if there is any relationship between possible inversion products and important reservoir factors, such as lithology and porosity. Fluid substitution was not attempted due to limited petrophysical logs available (i.e. no S-wave logs, estimated density and sonic logs). Well 24224 located southeast of the reef complex is analyzed

first, as it is the only well with both sonic and density logs (Figure 2.8). While it does not intersect the reservoir, cross-plotting the calculated Zp and Vp logs provide a good relationship between the laterally encasing A-2 Salt of the Salina Group and the carbonates within the Salina Group (Figure 2.9).

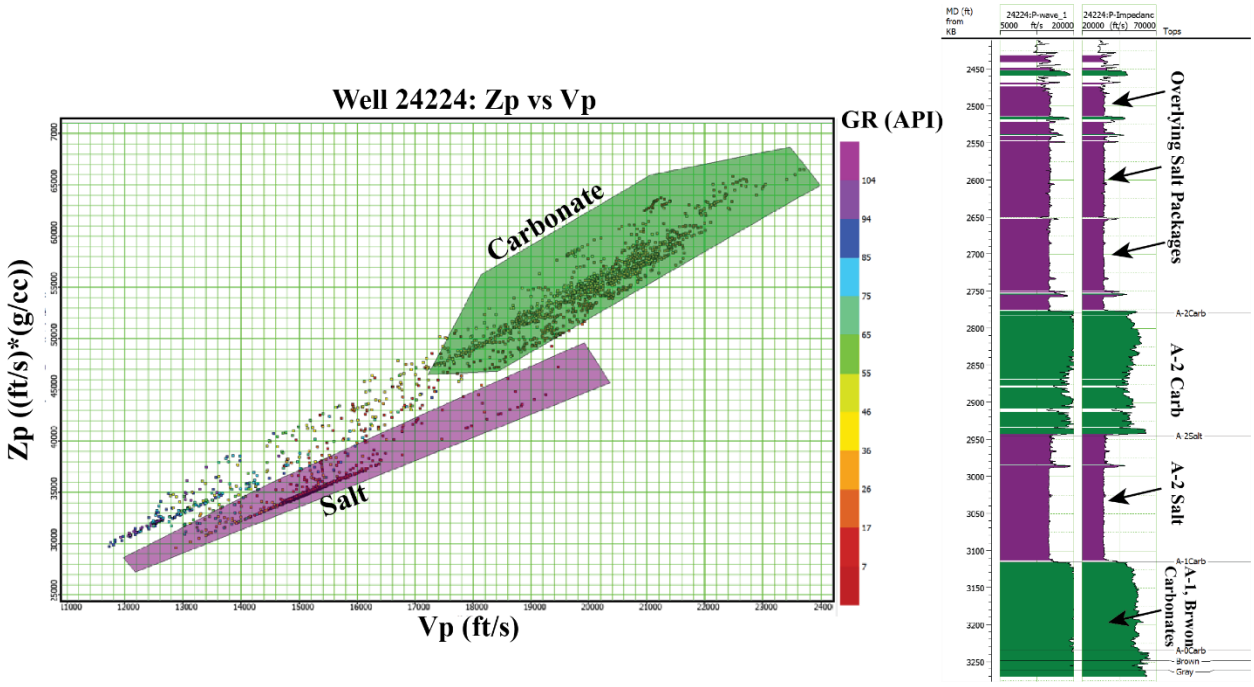

Figure 2.9: Zp vs Vp crossplot for Well 24224 located off of the reef. These attributes excel at differentiating salt from carbonate lithologies

The A-2 Salt is characterized by low Vp and Zp values, while the carbonates present have high Zp and Vp values. Well R-117 penetrates the reef core complex, and the Guelph Formation is 303 ft thick at this location. R-117 has core measured porosity and permeability logs throughout the entire Guelph Formation in addition to a measured P-wave sonic log. Density is estimated from the sonic log using Gardner's relationship, and then S-wave velocity is estimated using Xu et al (2007) workflow. The Vp/Vs ratio and Zp logs are cross plotted and data points are colored by porosity to analyze the relationship between velocity, density and porosity. It is apparent that

as porosity increases Zp and Vp/Vs decreases (Figure 2.10).

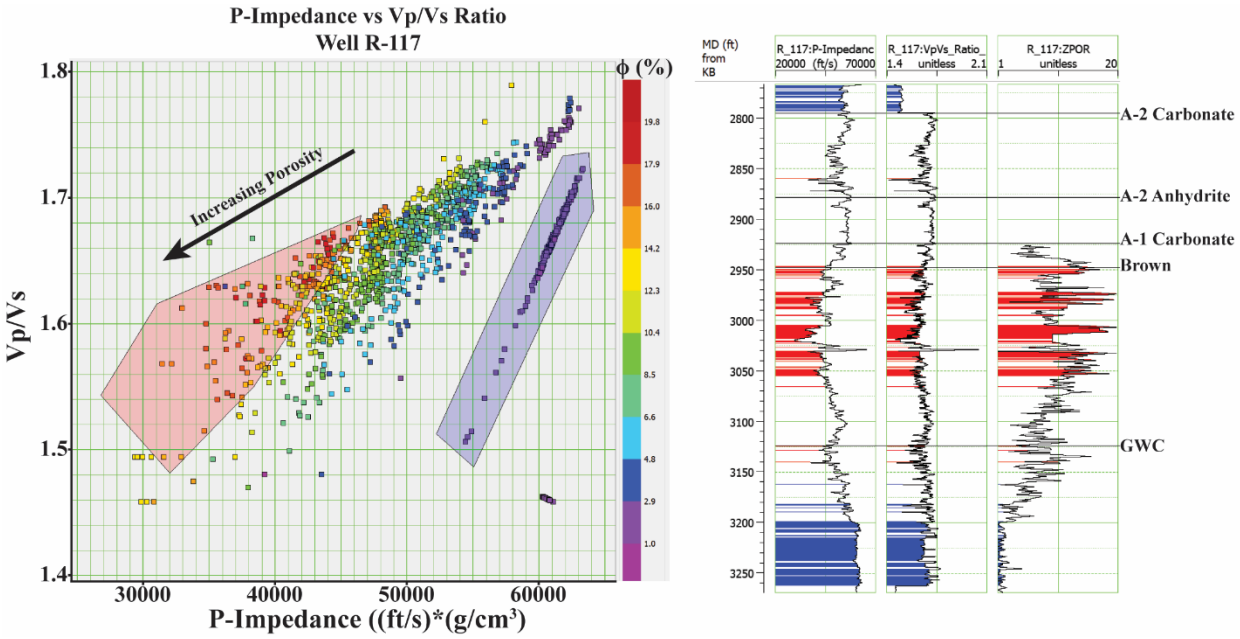

Figure 2.10: Crossplot of Vp/Vs and P-Impedance at well R-117 which intersect the reef core. Porous reservoir rock is delineated from tight non-reservoir rock, and a trend of increasing porosity with decreasing Vp/Vs and P-Impedance is observed.

Calculating lambda-rho mu-rho (LMR) logs following the method after Goodway et al. (1997) and cross plotting the logs indicates that LMR attributes can separate porosity as well within the reef core, as low LMR values correspond to high porosity zones primarily within the reef core above the gas water contact, and some subtle horizontal spread is present and can likely be

attributed to the effect of gas (Figure 2.11).

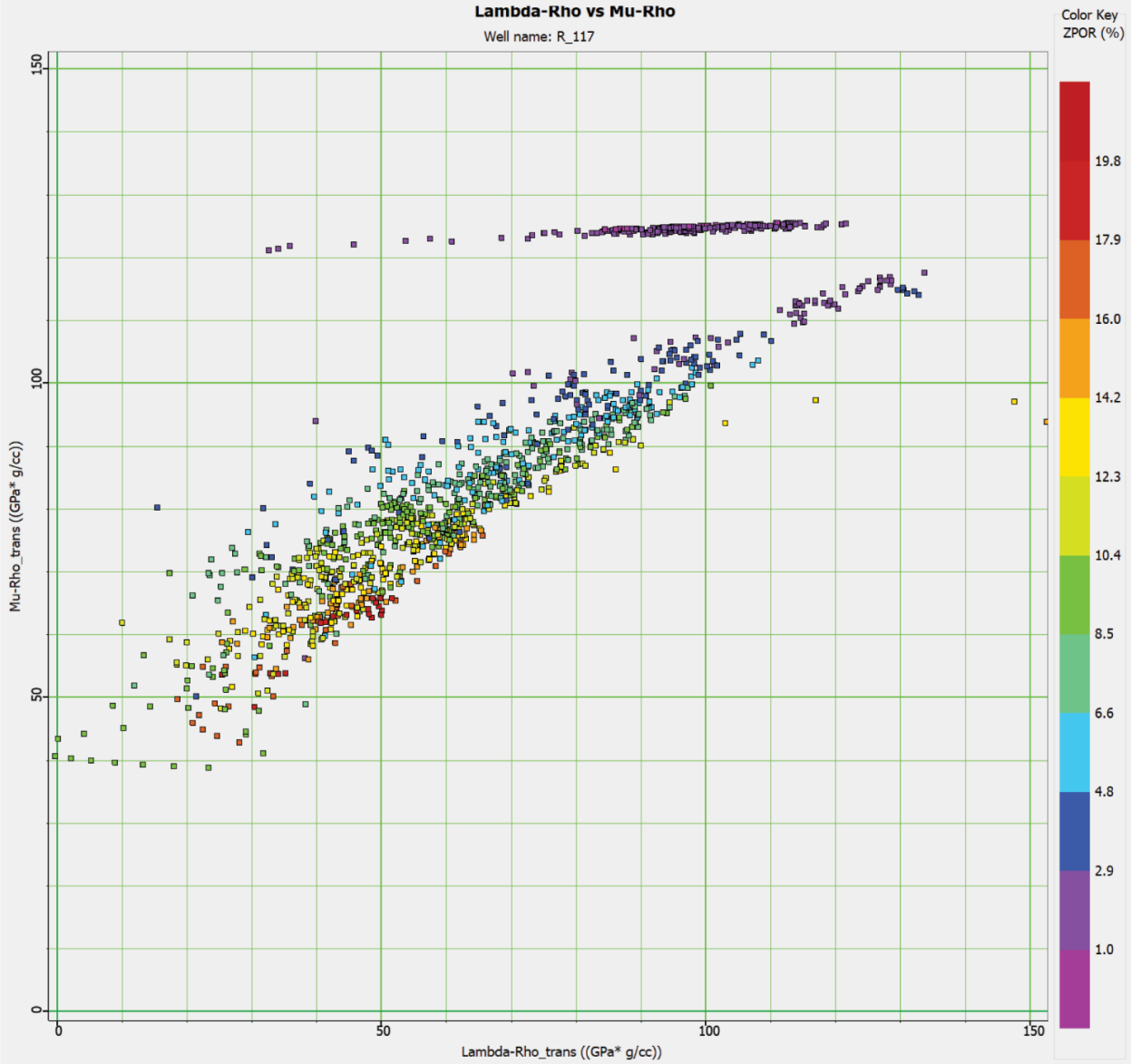

Figure 2.11: Crossplot of computed LMR values for well R-117. This crossplot enhances separation of porous and tight samples, as porous zones correspond to low LR and MR values.

Overall, the trends present are similar to those described by Goodway et al (1997) and Hoffe (2008). Relationships observed in the well logs confirm the feasibility to identify petrophysical properties from cross-plotting that correspond to high and low porosity zones using products attainable from a pre-stack inversion.

Results

Investigation 1: Inversion and LMR Analyses

The goal of conducting seismic inversion is to calculate quantitative measurements of the visualized subsurface which can be utilized to map changes in porosity, fluid content, or lithology (Chopra and Constagna, 2014). In this study, the goal is to attempt to understand the distribution of high quality reservoir zones, and enhance our understanding of why the zones are there.

Pre-stack Inversion Analysis

Figure 2.12 provides a comparison between the Zp volume from the pre-stack inversion and the geologic model for pinnacle reefs proposed by Rine (2017). A good correlation is observed between the Zp volume and the computed Zp logs in well R-117.

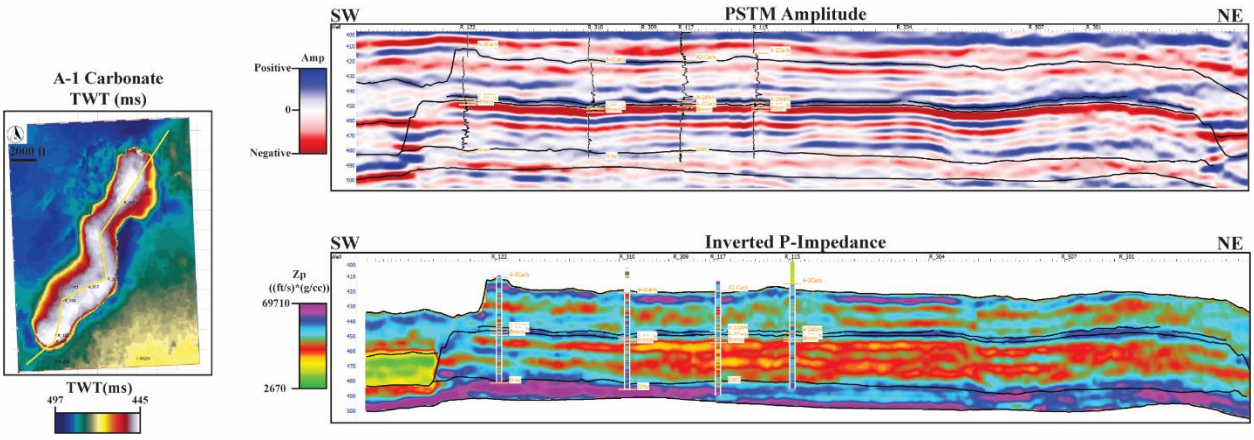

Figure 2.12: Comparison of the PSTM amplitude data through Ray Reef and the inverted P-Impedance volume.

Surrounding wells with estimated sonic and density logs have similar trends observed in the inversion result, but do not exactly match. This can be attributed to uncertainties associated with the calculated logs and their respective well-to-seismic ties. In post-stack amplitude data, Ray Reef is characterized by planar internal reflectors which decrease in amplitude toward the base of the

reef and become more discontinuous (Figure 2.12). Uncertainties arise when trying to interpret the extent of the reef core and bioherm and little geologic information can be extracted from the seismic amplitude directly. It is also difficult to differentiate the overlying A-1 Carbonate from the A-2 Anhydrite (Figure 2.12) from the seismic amplitude data due to the lack of acoustic impedance between anhydrite and dolomite lithologies. Well log data indicates that these units are just below the estimated resolution of the seismic data but should be detectable. The A-2 Anhydrite ranges in thickness from 30 to 50 feet and the A-1 Carbonate ranges from 30 to 45 feet thick above Ray Reef. By removing the effect of the wavelet and analyzing the Zp transect, the two units can now

be distinguished, as the A-2 Anhydrite is characterized by high Zp values due to its high density and Vp values (Figure 2.13).

Analyzing a cross-section through the reef crest and comparing that to the model of Rine (2017), similar layer geometries are observed (Figure 2.13). The A-2 Anhydrite correlates with the thin high Zp layer overlying the reef. Additionally, the lower porosity, more cemented reef bioherm

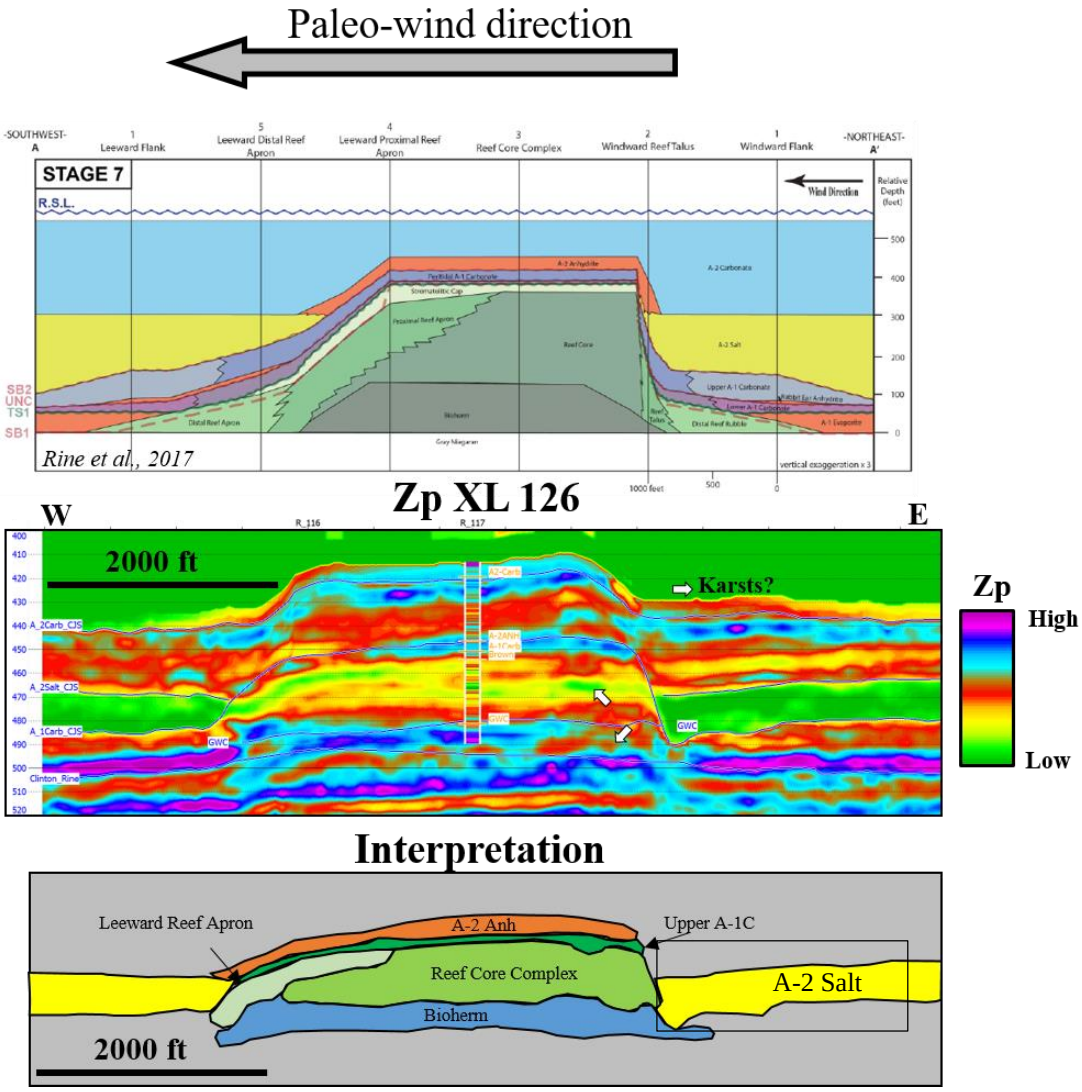

Figure 2.13: Qualitative interpretation of lithology from the P-Impedance attribute volume output from the pre-stack inversion. Similar geometries of isolated low to medium Zp values are observed within the reef complex as proposed by Rine (2017).

facies correspond to a region of high Zp values near the base of the reef. The reef core is characterized by mid to high porosity and lower Zp values. An onlapping band of low Zp values onto the reef core complex is interpreted as the proximal leeward apron (Figure 2.13). Potential localized karsts may also be indicated by semi-circular depressions of mid Zp values indicated by white arrows. These are approximately at two exposure surfaces, one between the peritidal stromatolite cap sequence at the top of the reef, and another at the top of the bioherm (Wold, 2008; Rine et al., 2020). Prior to the seismic inversion, interpretation of these depositional facies and potential karts was not possible from the PSTM amplitude data.

Lambda-Mu-Rho (LMR) attributes aim to transform P and S impedance values to values related to the Lamé constants to aid in determining rock and fluid properties (Goodway et al., 1997). Mu (μ) is the Lame parameter of rigidity and Lambda (λ) is the Lame parameter for compressibility. These parameters are dependent on a rock's velocity, porosity, and fluid content. The exploratory data analyses done indicates that zones with low LMR values correspond to porous (greater than 10%) zones, and porosity gradually decreases as LMR values increase (Figure 11). Using the pre-stack Zp and Zs volumes as input, Mu-Rho and Lambda-Rho volumes are calculated (Figure 2.14). When viewed independently, the reef core complex is characterized by low λρ and μρ values. Both attributes also visualize the overlying A-2 Anhydrite and reef bioherm well and both are represented by high values in each attribute. This correlates well with well log observations of these units, as the A-2 Anhydrite has higher measured density values, as well as

measured sonic values.

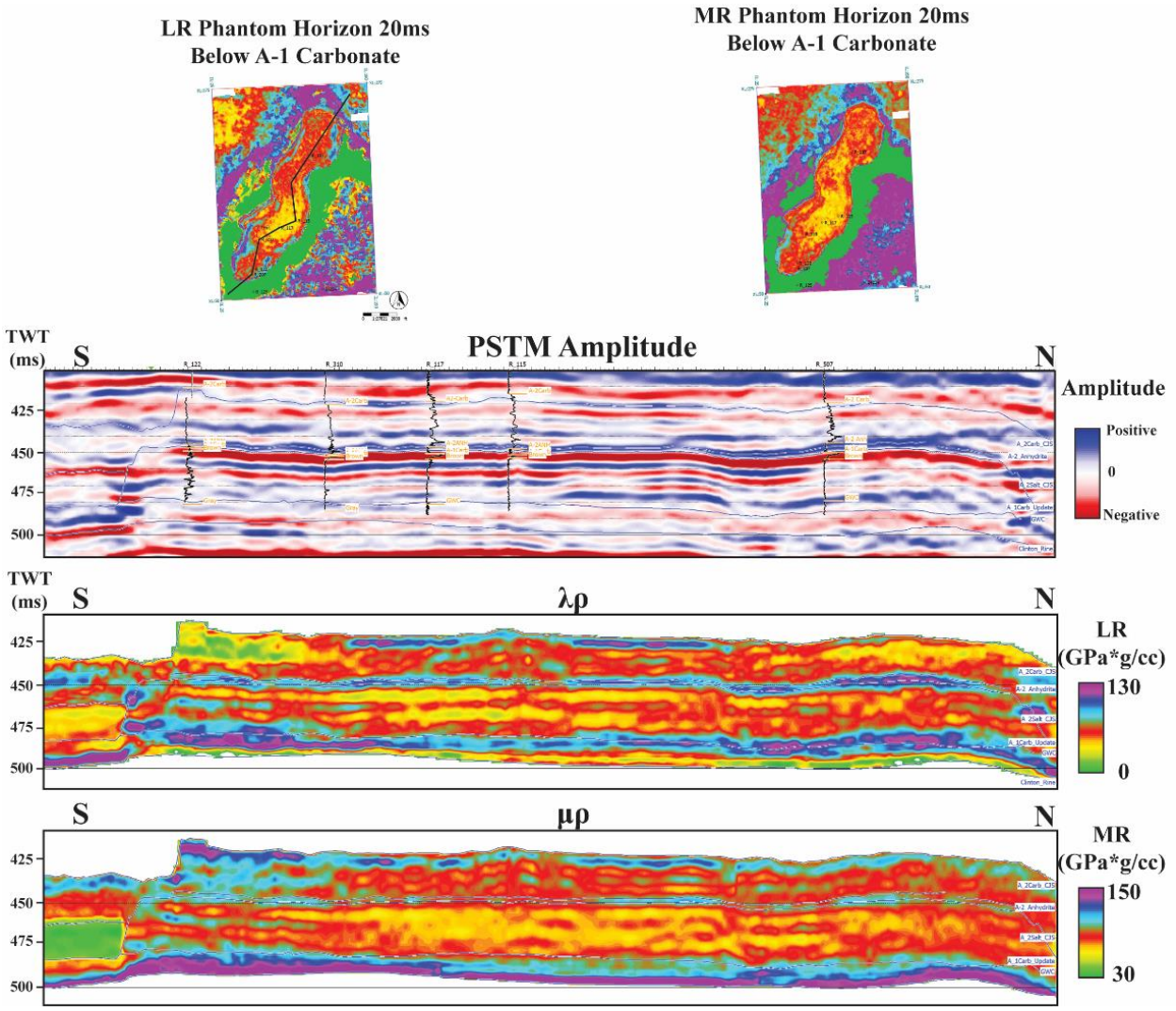

Figure 2.14: Comparison of the PSTM amplitude data and the LR and MR attribute volumes computed from inversion attributes A fairly consistent distribution of low LR is observed, with minor alternating layers of high LR. The MR volume is primarily low values throughout the central portion of the reef, with high MR values present in the South.

While the bioherm has similar density values as the reef core complex, the measured sonic logs are typically higher due to the decrease in porosity within the bioherm. The bioherm is also typically below the GWC, and the presence of water would result in an increase in λρ values as it is less compressible than gas. The onlapping A-2 Salt is also characterized by low λρ and μρ values, similar to the reef core complex. To remove data points belonging to the A-2 Salt, a Zp

vs. Vp crossplot is used to classify voxels belonging to the salt unit following the relationship observed in well 24224 shown in Figure 2.9 (Figure 2.16). The relationships seen in the well logs is observed in the seismic and classifies the A-2 Salt well.

Cross plotting the λρ and μρ volumes and using the Hoffe (2008) LMR template as a background guide, the LMR attribute crossplot has similar relationships as those observed in the

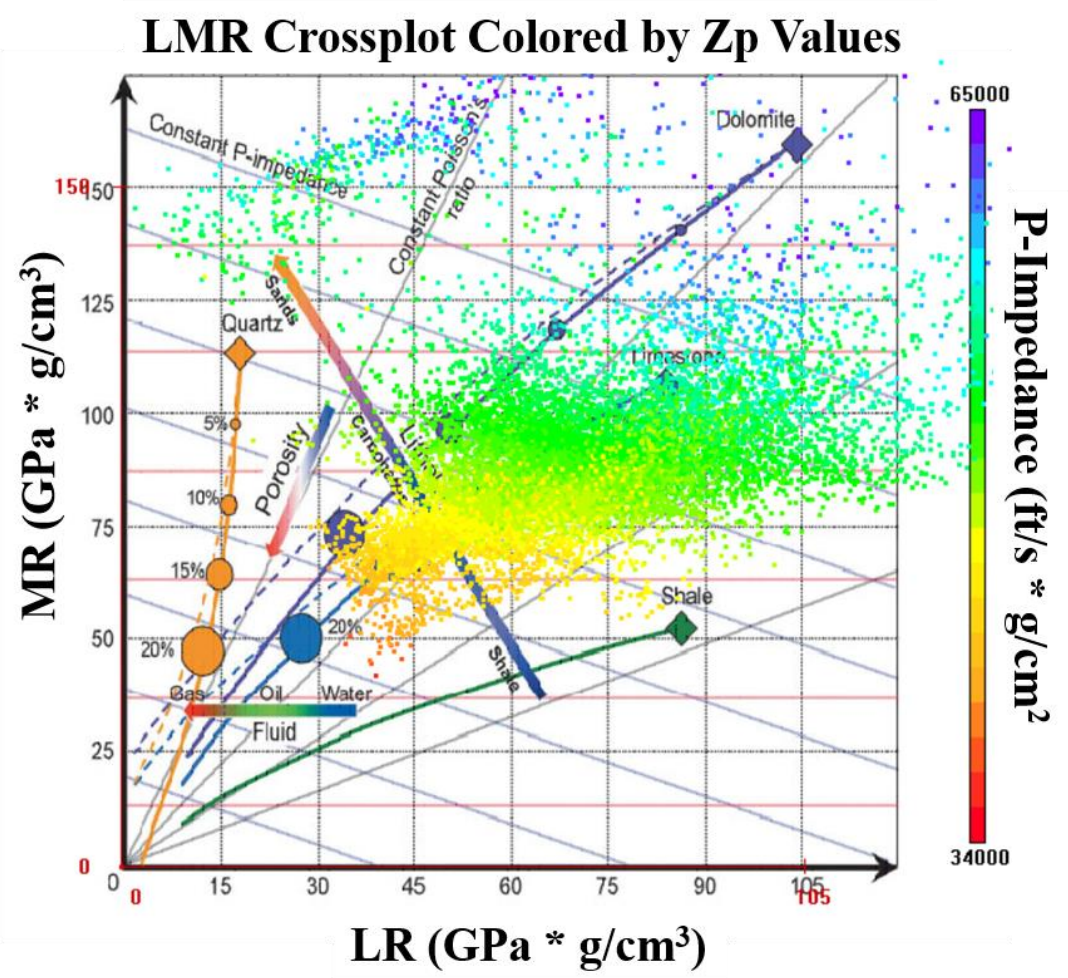

Figure 2.15: Crossplot of LMR colored by Zp values. The inserted background guide is proposed after Hoffe (2008). The calculated LMR volumes follow the proposed trends, with almost all of the data points plotting within the values for dolomite and limestone.

background template. The majority of data points plot within the bounds of limestone and dolomite lithologies, and diagonal lines connect data points with constant P-impedance (Figure 2.15). Data

points from the inversion volumes plot within the proposed region for carbonate lithologies. In addition, coloring the data points by their P-impedance values shows that values with similar P-impedance plot along diagonal lines. As $\lambda\rho$ and $\mu\rho$ attributes are typically cross-plotted to identify zones of favorable porosity and fluid content, seismic facies will be defined from user defined polygons from the LMR crossplot. Investigation boxes are drawn at cored well locations at intervals of good, fair, poor, and tight porosity and their corresponding data points are highlighted in the LMR cross plot. Polygons are then picked around these data points, and iteratively adjusted to best match other well data. During the classification workflow, it became apparent that possible fluid effects were present in $\lambda\rho$ values within zones of good and fair porosity, and these were sub-classified from each respective class. Figure 2.16 shows the final classified seismic cube and crossplot. The classification provides a patchy and heterogeneous distribution of the good porosity, gas prone seismic facies that is intersected by high-porosity wells, and not located at zones of low porosity (Figure 2.16). A broad laterally consistent and vertically layered distribution of good and fair porosity zones are classified within the reservoir interval in the reef. This distribution of predicted porosity in broad layered zones is consistent with well-based geostatistical models previously published on Ray Reef (Wold, 2008; Haynie, 2009) (Figure 19). The lowermost part of the reservoir, the bioherm, is classified as predominately tight porosity, which is correct in some well locations (R-117) while incorrect in others (R-109). The LMR classification did not detect any zones of high porosity within this interval, which may be attributed to a limited amount of wells which log this interval. Wold (2008) used a sequence stratigraphic approach for rock type classification from core analysis, and the resulting petrophysical models have a stratified distribution of porosity values with cyclical layers of low to high porosity (Figure 2.17). While the seismic data is not high enough resolution to capture the fine-scale cyclicity, it captures the large

scale cyclicity with a good-fair-good stacking pattern of porosity classifications. Haynie's (2009) approach of defining petrofacies (rock types based on similar petrophysical properties) resulted in models that honored the heterogeneities present within the formation through stochastic modeling methods and variography (Figure 2.17). While heterogeneous, a broad and consistent distribution of porous facies was observed, similar to the results of this study (Figure 2.19). One discrepancy

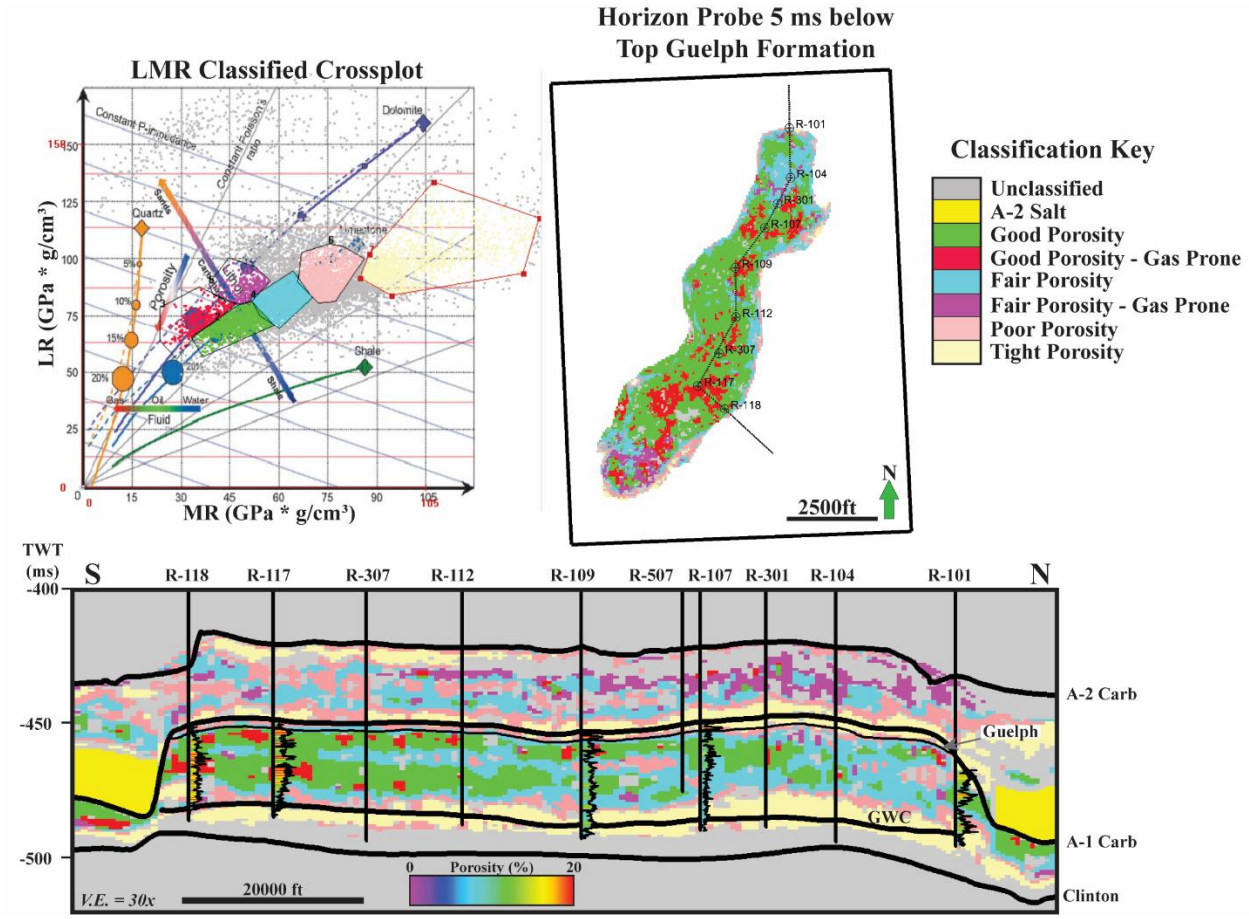

Figure 2.16: Classified seismic facies volume of Ray Reef using LMR attributes. Good porosity correlates to greater than 10% porosity, fair porosity is 5 to 10%, poor porosity is 2 to 5% and tight is less than 2%.

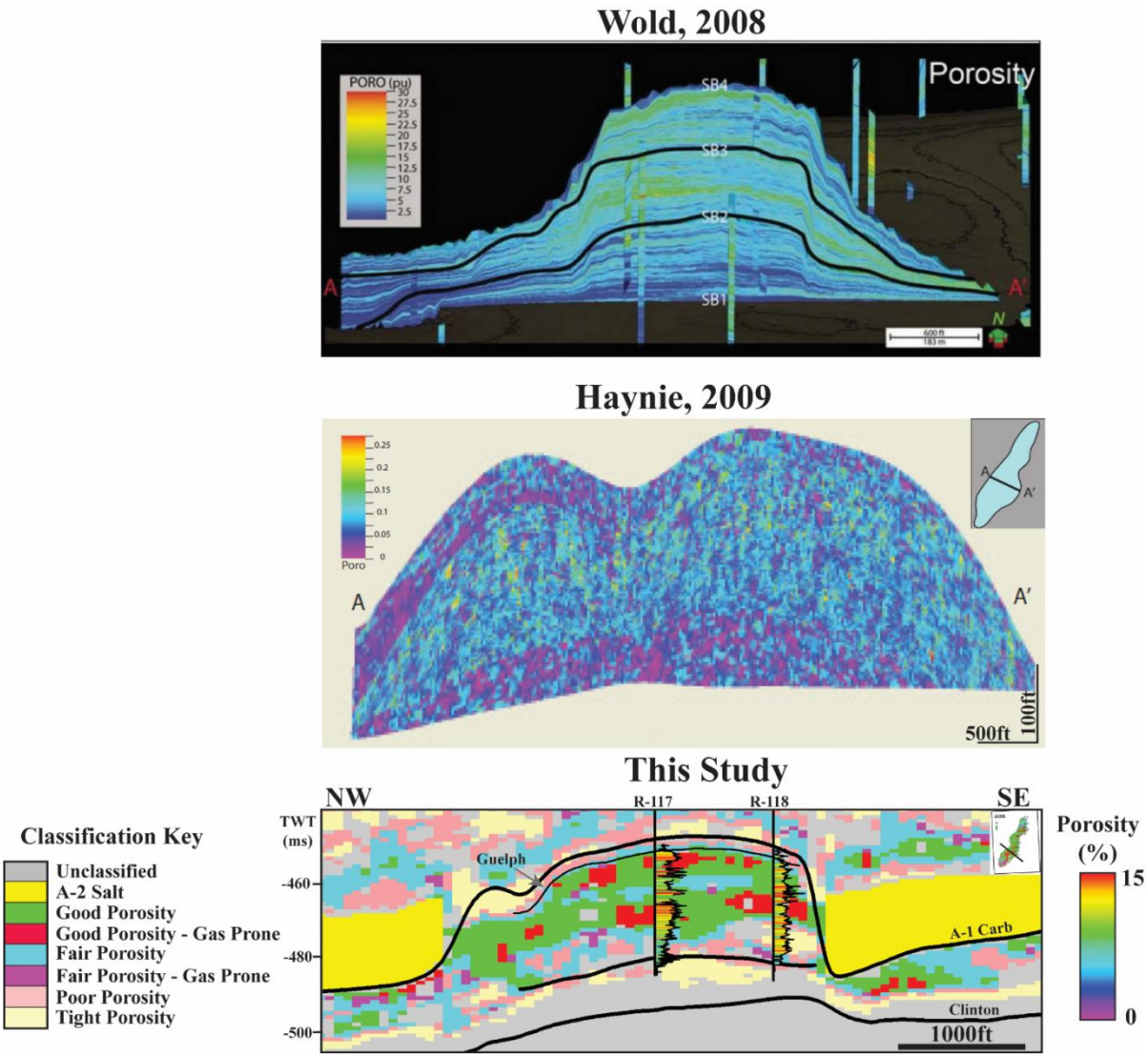

Figure 2.17: Comparison of the classified seismic facies using LMR attributes to two previous studies of Ray Reef. Wold (2008) utilized a sequence stratigraphic approach for defining depositional facies. Haynie, 2009 based their model on petrofacies – lithologies with similar petrophysical and depositional attributes. The classified volume is displayed with core porosity logs overlain.

between this seismic-based study is that both well-based studies found a limited amount of porous dolomite within the bioherm interval. Another is that the small-scale heterogeneity observed in core data was not captured by the seismic facies. Overall, the LMR classifications within the reef core reservoir correlates well with previous geostatistical models of ray reef as similar trends in porosity are observed.

To analyze how the classified porosity seismic facies correspond to the measured well logs, a map of storage capacity was calculated. Two geobody extractions were done: the first extracted all voxels within the good porosity facies, and the second with the fair porosity facies. Horizons were draped over the top and base of each geobody, and an isochron was computed for each respective pair of horizons. The isochron values were then multiplied by the corresponding porosity value for each facies (0.12 for good porosity; 0.7 for fair porosity). These maps were then

added together to create the final storage capacity map for Ray Reef (Figure 2.18a).

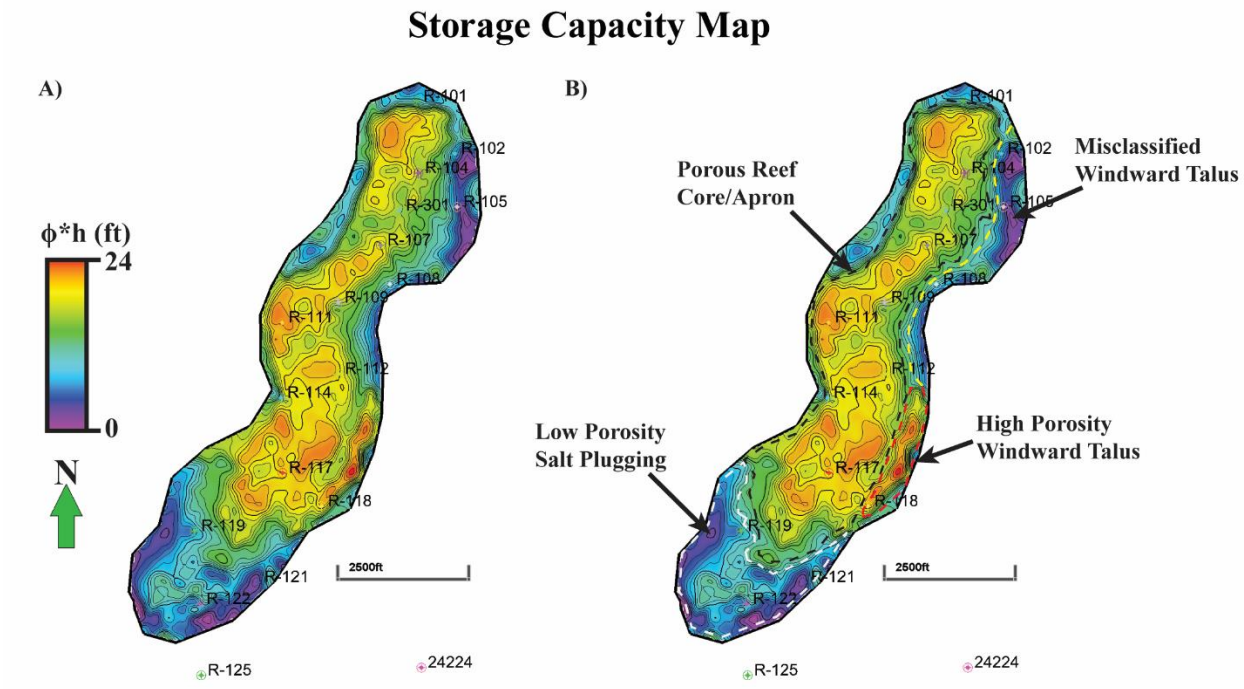

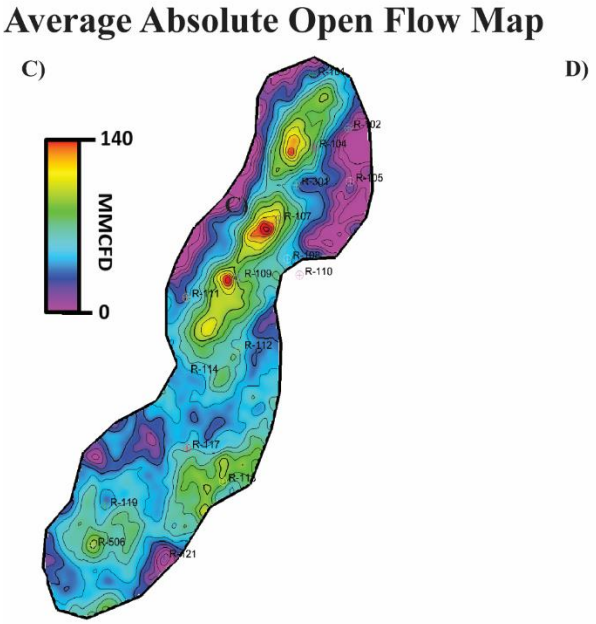

D)

Well	Mean ϕ*h (ft)	Predicted ϕ*h (ft)	Error
R-101	14	13.2	-6%
R-102	14.4	11.1	-23%
R-104	22.5	18	-19%
R-105	12.2	9.0	-26%
R-107	20.7	19.8	-4%
R-108	26.4	11.65	-55%
R-112	18.2	20.66	+13%
R-114	15.3	16.9	+10%
R-117	24.3	21.6	-22%
R-118	28.7	22	-24%
R-119	3.2	9	+181%
R-121	7.55	5.5	-27%
R-301	10.2	17.4	+70%

Figure 2.18:A- Storage capacity map computed for Ray Reef from the classified seismic facies. B- Interpreted storage capacity map. C- Average Absolute Open Flow map of Ray Reef generated using observation data from 40 wells within Ray Reef. D - Table displaying the mean storage capacity of wells with measured porosity data and predicted storage capacity from the classified seismic facies model generated in this study.

The storage capacity map displays high porosity zones within the central reef core and northern reef talus apron. Porous zones associated with windward talus deposits are also captured by the storage capacity map along the southeastern margin of the reef. The porosity model misclassifies the porous northern windward talus deposits as low porosity where core porosity values in wells R-105 and R-108 indicate these are high-porosity zones (Figure 2.18b). The southern reef core is characterized by low storage capacity, and core data suggests that this is due to partial salt plugging of the pores in this region (Figure 2.18b). Comparing the interpretations from the storage capacity map to the Average Absolute Open Flow Map, which shows well flow performance independent of subsurface conditions, suggests good qualitative correlation within the northern region of Ray Reef (Figure 2.18c). This indicates that while having good storage capacity is key for good well performance, other factors can influence well flow as the south-central portion of the reef exhibits good storage capacity but poor flow. These pores may be more isolated and disconnected, thus inhibiting flow. Figure 2.18d displays the correlation between the mean storage capacity of cored wells and the computed storage capacity from the classified seismic facies model. The overall average error for all wells is 37%, however wells R-119 and R-301were partially cored. R-119 only cored the reef bioherm, which accounts for the large over-prediction of storage capacity. Well R-301 was cored for 130 ft whereas the reef is approximately 310 ft thick in this location. Only using the fully cored wells, the average error decreases to 21%. This lower error provide promising correlation between the classified porosity facies and well data, and indicates the seismic data is capturing the large scale trends.

Investigation 2: Rock Type Classification from Seismic Data

Understanding the distribution and structure of the reservoir lithofacies is a key aspect of reservoir modeling that will influence petrophysical modeling. Being able to predict or calculate a probability volume for rock type or lithofacies away from well locations using seismic data can serve as valuable input in reservoir modeling (Tellez et al., 2021). This investigation comprises of two workflows that aim to use machine learning techniques to classify rock types within the Ray Reef gas storage reservoir. The first applies the unsupervised GTM algorithm above to post-stack seismic attributes and the second study applies a supervised PNN to extrapolate rock types classified from porosity and permeability logs to seismic data.

2.1: Generative Topographic Mapping (GTM)

Commonly, pre-stack seismic data is not available for a variety of reasons. Without pre-stack conditioned gathers, the amount of information we can solve for through inversion is limited to P-impedance and AVO studies are not possible. Using the GTM algorithm described previously, the goal for this study was to identify seismic facies from clusters in the post-stack GTM result and relate those to the geologic or petrophysical properties of the reservoir. To overcome the limitations of post-stack seismic data, we begin by investigating the data corresponding to the cored well R-107 and extrapolate classifications to other cored wells. As seismic data has limited vertical resolution, the multiple depositional facies described in Rine et al's (2017) reef model were lumped into three main facies: the bioherm, reef core complex, and overlying peritidal facies.

The input seismic attributes were chosen based off previous studies and interpreter experience. Previous studies over southern Niagaran reefs investigating unsupervised machine

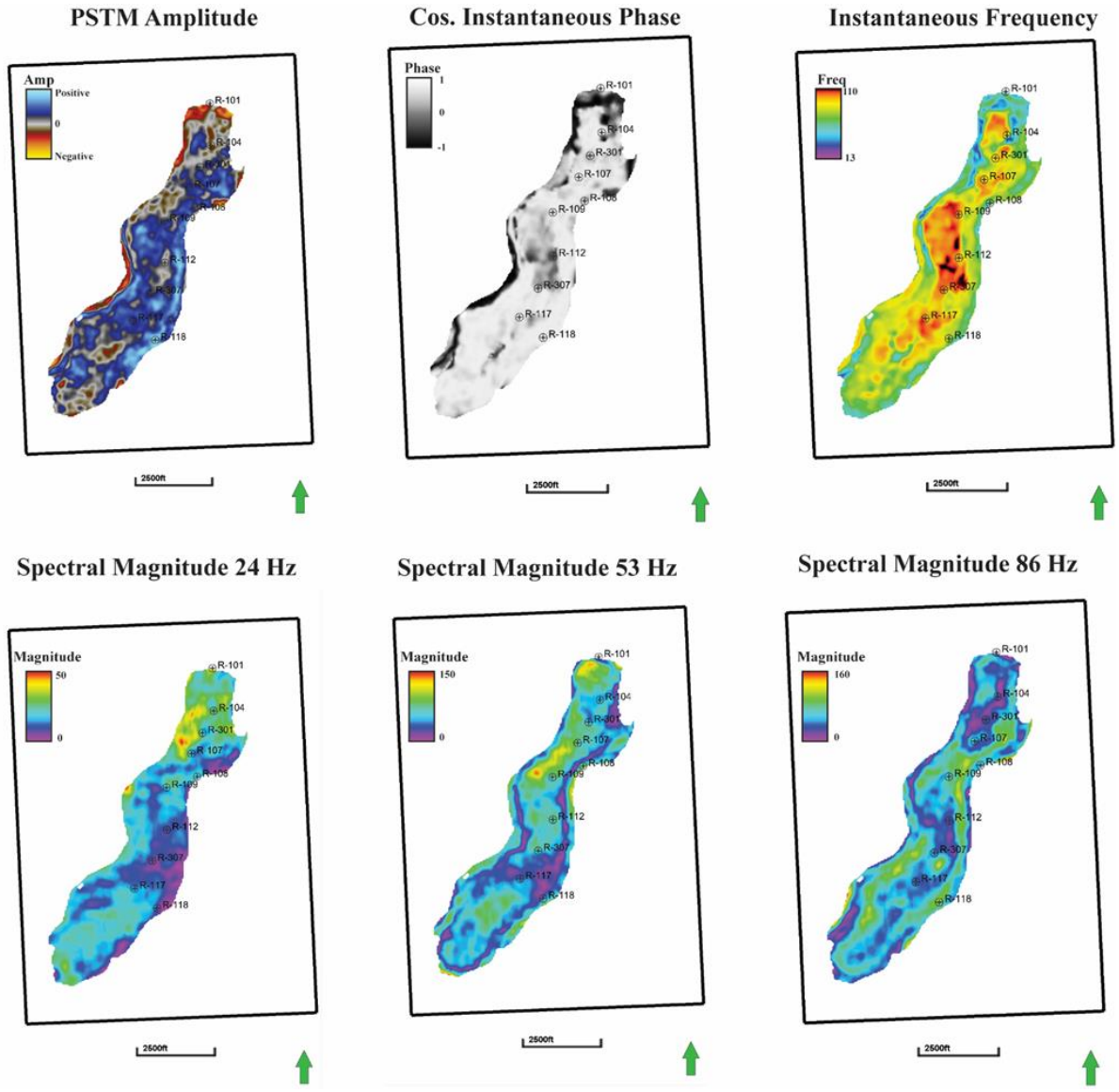

Figure 2.19: Summary of the input attributes for the GTM. Each attribute is extracted 15 ms TWT below the top of the A-1 Carbonate, and is representative of the reef core complex of the Guelph Formation.

learning techniques applied to seismic data have identified that frequency-based attributes have the potential to differentiate high and low porosity zones from volume attributes (Buist, 2020). Figure 2.19 provides an overview of the attributes used as input for the GTM. This included:

Instantaneous frequency, cosine of instantaneous phase, and iso-frequency volumes output from spectral decomposition. Within the reef core, the cosine of instantaneous phase attribute has an anomalous negative phase zone near the central portion of the reef, which may indicate a stratigraphic change. The portion of the reservoir mapped by the phantom horizon is mostly positive, with negative values around the western and northern margins (Figure 2.19). Instantaneous frequency is the time derivative of instantaneous phase. Low instantaneous frequency values have been shown to correlate to high porosity zones within Niagaran reefs along the northern reef trend (Toelle, 2018). The zone of negative instantaneous phase correlates strongly with high instantaneous frequency values, and core data from wells R-117 and R-107 indicate this is a zone of high porosity in both wells. This calls into question the validity of the relationship between instantaneous frequency and porosity, however the attribute does reveal subtle changes within the reservoir. Three iso-frequency cubes from spectral decomposition were also used as input. The extractions of the 24, 53, and 87 Hz frequency components are displayed, and each reveals features unique to those frequencies (Figure 2.19). The 24 Hz displays a relatively weaker magnitude response, however the low frequency captures strong responses in the northern part of the reef not seen in the higher frequency components. The 53 and 86 Hz components both image internal variations in frequency and possible heterogeneities present within the reservoir interval. The margins of the reef complex are represented by a weak response in the 53 Hz and a strong response within the 86 Hz, which may be due to tuning effects related to thickness (Figure 2.19). Individually, the attributes reveal subtle clues about the reef complex, but are difficult to directly link to lithology or reservoir quality.

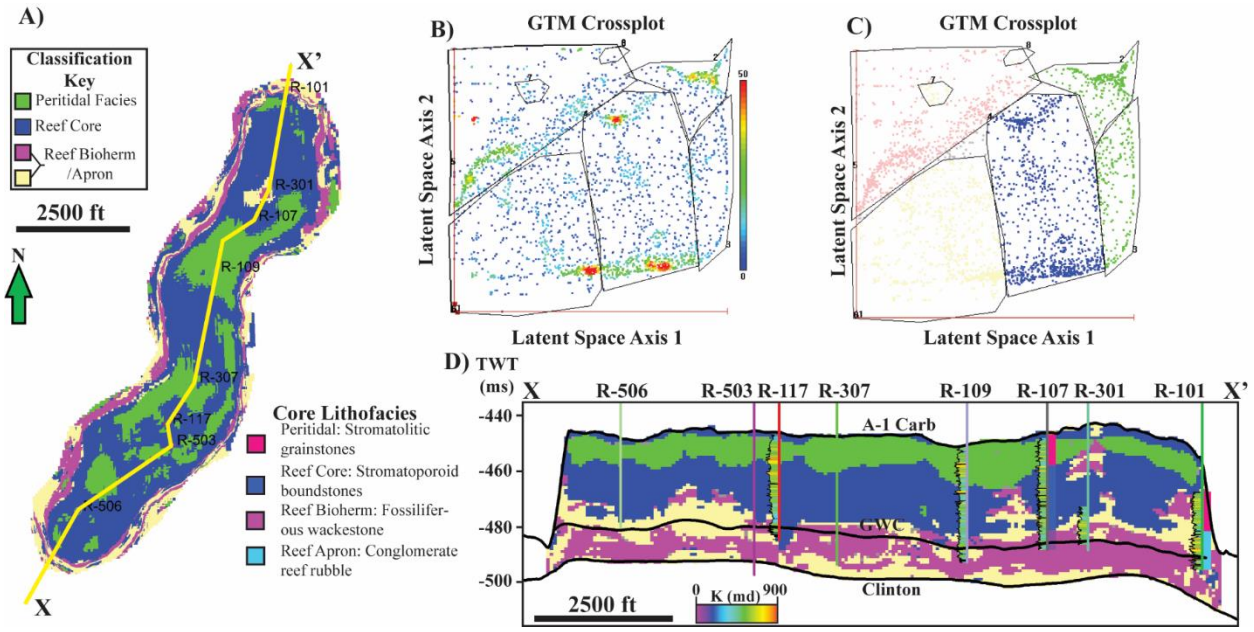

Figure 2.20: A- Phantom horizon 15 ms TWT below the top A-1 Carbonate. B- Classified crossplot colored by point density. C- Classified crossplot colored by class. D- Arbitrary line through the classified volume.

The full angle stack classification is shown in Figure 2.19. The top A-1 Carbonate horizon is shifted down 15 ms to create a phantom horizon. This horizon has the same geometry and TWT structure as the A-1 Carbonate horizon and is 15 ms below the original A-1 Carbonate horizon. This phantom horizon displays the classified volume approximately through the top of the Guelph ("Brown Niagaran") Formation (Figure 2.20a). The crossplots of the two latent space axes volumes display the data corresponding to the cross-section shown below (Figure 2.19d). Using the workflow described above, the polygons were initially centered about the clusters, and calibrated to the wells with core lithology logs. This resulted in a good match of the overlying peritidal facies and reef core complex at cored wells within the reef complex. However, the reef bioherm is poorly discriminated from the reef apron and talus facies as seen in well R-101. There is also an anomalous classification of Bioherm/Apron facies in the upper section of well R-301. The arbitrary line through the reef suggests that Ray Reef is composed of three bioherms that

likely amalgamated together through growth, which then acted as the substrate for subsequent reef growth.

As the reef core complex is the primary reservoir target, and the best classified seismic facies by the GTM, further analyses focused on quantifying reservoir thickness away from well locations. A geobody extraction was done for the reef core seismic facies (Figure 2.21) by inserting a horizon probe into the discretized volume (Figure 2.21). To ensure an accurate

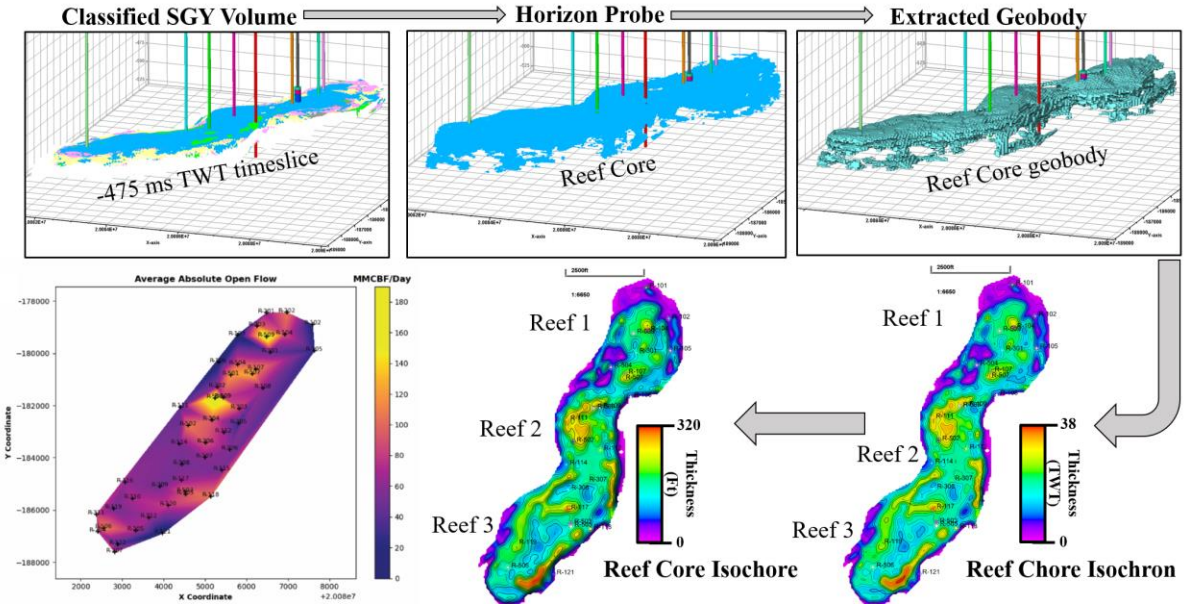

Figure 2.21: Top row: Evolution from the classified volume to a voxel-based extraction for the Reef Core seismic facies defined from the GTM. Bottom Row: The Reef Core isochron is converted to an isochron, and is a representative reservoir thickness map. High AAOF values correlate to anomalously thick reservoir zones.

extraction, the visible extents of the horizon probe used for the extraction was limited to avoid extraction of mis-classified facies at the top of the A-1 Carbonate horizon. Surfaces were then wrapped along the top and base of the extracted geobody. An isochron was calculated by subtracting the base surface from the top. Using the sonic log from well R-117, an average interval velocity of 19,500 ft/s was used to transform from TWT thickness to thickness in feet

(Figure 2.21). A map of average absolute open flow (AOF) was produced using a simple interpolation algorithm (Figure 2.20). It becomes apparent that the northern and central reef complexes exhibit good flow performance, while the southern reef complex has average to low flow performance. Comparing the AAOF map to the isochore created from the geobody extraction, it is clear that wells that encounter thicker intervals display better flow performance. As the reef core lithofacies are characterized primarily by broad, stratified layers of porous dolomite, the wells which penetrate the thickest portions of the reef core are likely to perform the best.

Unsupervised classification of seismic facies was accomplished by applying generative topographic mapping to post-stack seismic attributes in a pinnacle reef gas-storage reservoir with vintage well control. The reef core and overlying peritidal facies were well classified which allows for quick mapping of their respective morphologies. The bioherm and flanking facies were difficult to discriminate. This may be attributed to the poor imaging of the flanks of the reef complex due to their steep dips and velocity pull-up. Quantification of reservoir thickness from seismic data was accomplished through extracting geobodies from the classified reef core facies, and applying a constant interval velocity.

Investigation 2.2: Identification of Hydraulic Flow Units from Seismic Data

Direct measurements of porosity, permeability, mineralogy, and pore structure from subsurface reservoirs of porosity and permeability can give geoscientists and engineers a thorough understanding of the reservoir. Being able to relate porosity to permeability, especially in heterogeneous lithologies such as dolomite and other carbonates is often a challenge due to the complexities imposed by diagenesis and post-depositional deformation (Amaefule 1993; Pranter et al 2005). Diagenesis and dolomitization can result in the complete replacement or destruction

of the original rock fabric, which makes relating porosity and permeability – key reservoir properties – to lithology difficult. Amaefule (1993) proposed a methodology which identifies the classification of distinct hydraulic units within reservoir zones with similar flow performance, termed hydraulic flow units (HFU's). The theory of HFU's is based on the Kozeny-Carmen equation and mean hydraulic radius. The Kozeny-Carmen equation models fluid flow pathways as a bundle of capillary tubes, and applies Poisseuille's and Darcy's Laws to formulate a relationship between porosity and permeability. Amaefule (1993) derived two new variables from the Kozeny-Carmen relationship, Reservoir Quality Index (RQI) and the Flow Zone Indicator (FZI). RQI is defined as $RQI(\mu m) = 0.0314\sqrt{\frac{k}{\phi_e}}$, and FZI is defined as $FZI(\mu m) = \frac{RQI}{\phi_z}$, where k is permeability in milidarcies, ϕ_e is the effective porosity, and ϕ_z is the pore volume-to-grain ratio. Using the equation $logRQI = log\ \phi_z + logFZI$ and using a log-log plot of RQI and ϕ_z, samples with similar FZI values will lie on a linear line with a unit slope. Samples which lie on the same line will have similar pore throat attributes, and therefore make up a distinct hydraulic unit (Amaefule 1993; Prasad, 2003).

FZI values were calculated within Ray Reef using core measured porosity and permeability values from 14 wells which intersect the reservoir (Figure 2.22).

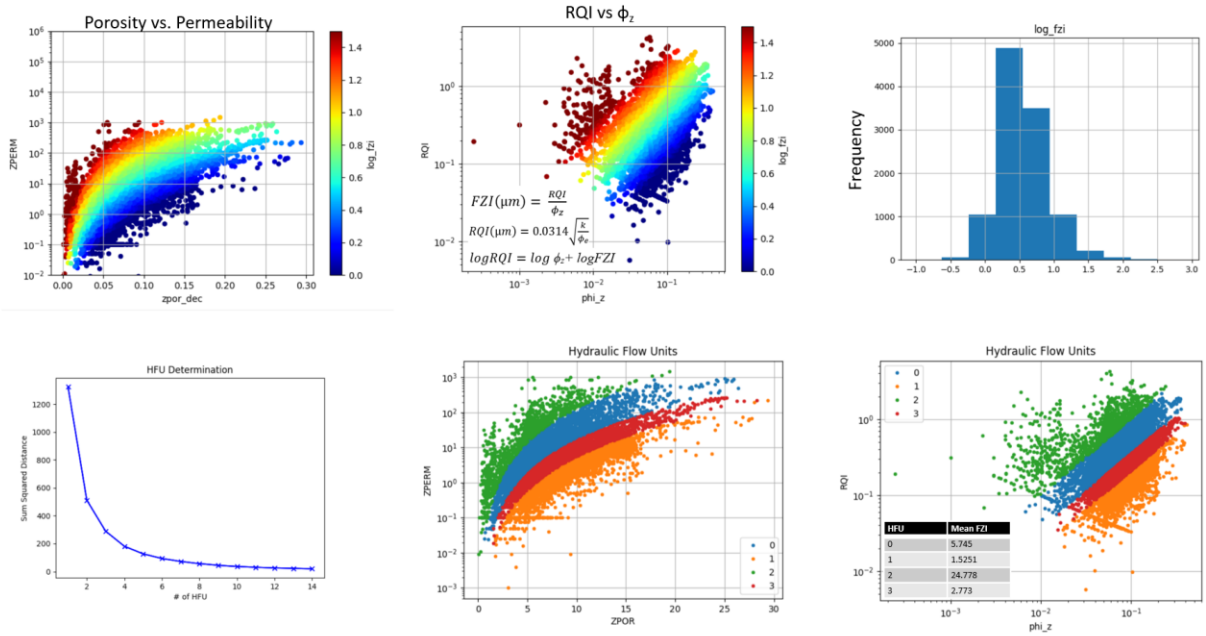

Figure 2.22: Series of plots displaying the defined Hydraulic flow units (HFU's). Note the linear trend of Log(FZI) values on the RQI-PHI_z plots.

While the aim of this study was to predict these flow units away from well locations utilizing seismic data, this workflow was not successful (Figure 2.23). Supervised neural networks were trained utilizing pre-stack inversion attributes generated in Investigation 1,

however no robust network could be trained (Figure 2.23).

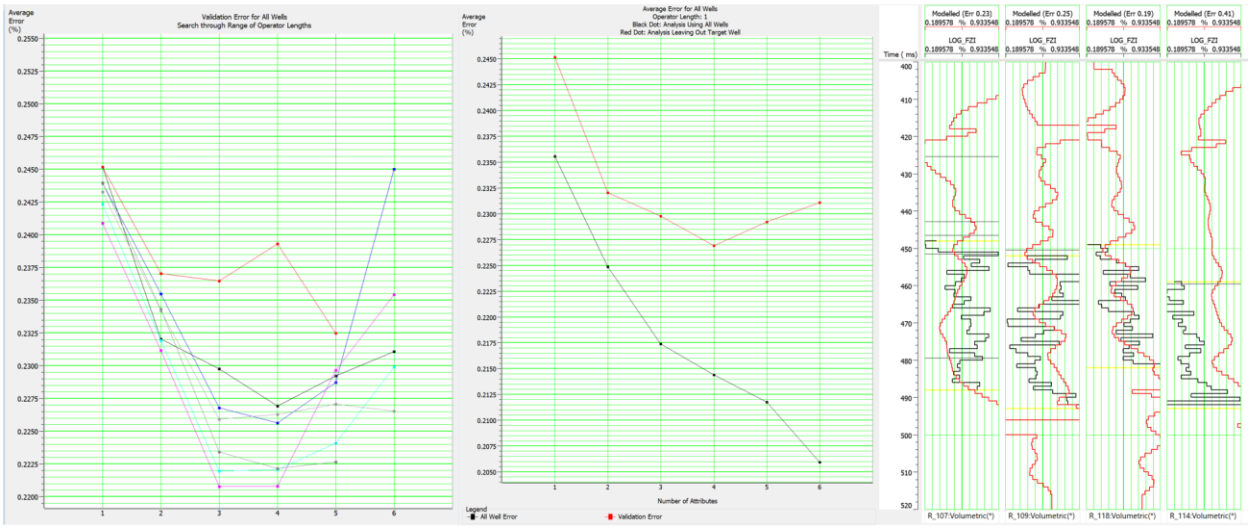

Figure 2.23: Multiattribute analysis for log FZI prediction from seismic data to find optimal combination of attributes and operator length. When validated on blind wells, the prediction fails.

The neural network failed during validation, regardless of the architecture used (PNN, MLFN, DFFN). The failure is attributed to a poor depth-to-time relationship within the cored wells. Many cored wells lack a measured sonic or density log, and require a manual time-to-depth conversion utilizing formation tops and seismic surfaces. This problem is compounded as none of the cored wells penetrate the underlying Clinton Formation, so the TD of the wells in TWT is uncertain as well. Another challenge this workflow faces is that many of these HFU's are well below seismic resolution. Resolution of the post-stack seismic data is approximately 40 ft. Many of the fluctuations of HFU's are on the order of one to five feet. Attempting to find relationships between these small-scale changes is a challenging prospect, and this is amplified by the poor time-to-depth relationship. A final possible issue is that no seismic attributes in Ray Reef are sensitive to changes in permeability.

Investigation 3: Probability Neural Network

3.1: GWC Classification

Utilizing supervised machine learning techniques is a powerful tool for classifying seismic facies that can provide a measure of confidence in the results (Lubo-Robles et al., 2021). The gas-water contact (GWC) in the Ray Reef field is not observable utilizing AVO analyses, as there is little variation in amplitudes, or conventional AVO attributes, with offset or angle. Additionally, the complex and heterogeneous pore structures documented within Ray Reef (moldic, vuggy, fracture etc.) identified by Trout (2012) indicate that Gassmann's Theory for fluid substitution is not valid for Ray Reef, preventing accurate rock physics and AVO modeling (Gassman, 1954) (Figure 2.24). This study aims to classify the GWC utilizing attributes from the pre-stack seismic inversion accomplished in Investigation 1. In the Hampson-Russell

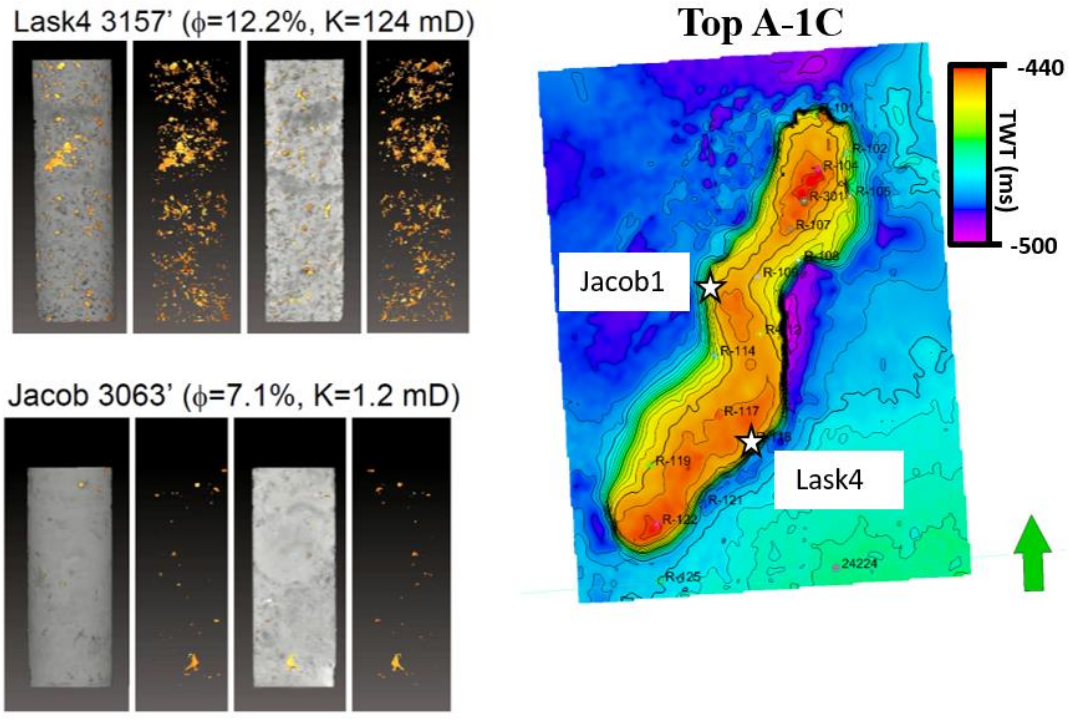

Figure 2.24: Examples of pore type heterogeneity within Ray Reef from Trout (2012). CT scans of two core samples reveal the pore geometries in three dimensions, which fail Gassman's assumptions.

simultaneous inversion workflow, it was apparent that a misfit was present at the GWC in well R-117 during the inversion analyses (Figure 2.24). The resulting inversion attributes (Zp, Zs, and VpVs) all over estimated their respective values at the GWC. The residual volume attributes output from the inversion display a high positive residual approximately at the GWC surface

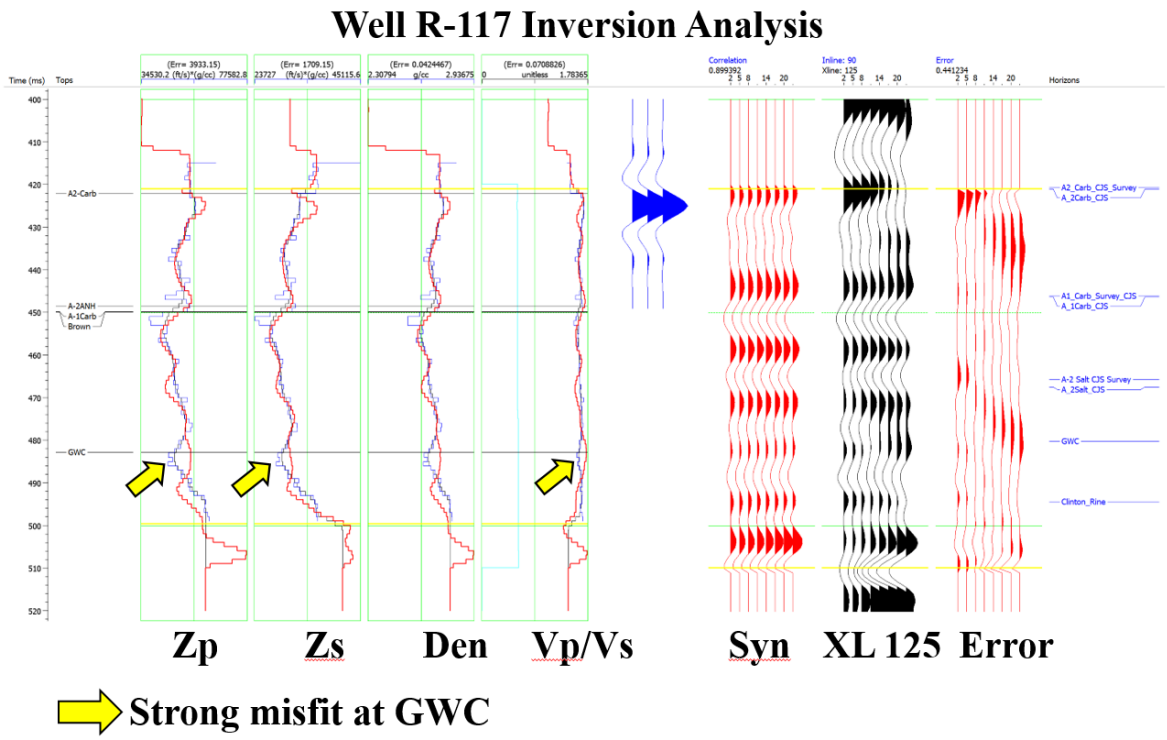

Figure 2.25: Inversion analysis for Well R-117 displaying the anomalous misfit at the gas water contact. The GWC was not used as an input surface in the inversion workflow.

provided by Consumers Energy which was sourced from well log picks (Figure 2.26). To create a training data set, training data in the form of polygons were picked on inlines and crosslines on a 10-line spacing. Two facies were picked: facies 1 corresponds to the GWC. This was picked on the Zp residual volume and was limited to the zone of high residual Zp at the base of the reef (Figure 2.26). Facies 2 was designated as “Not GWC” and polygons were picked on within the

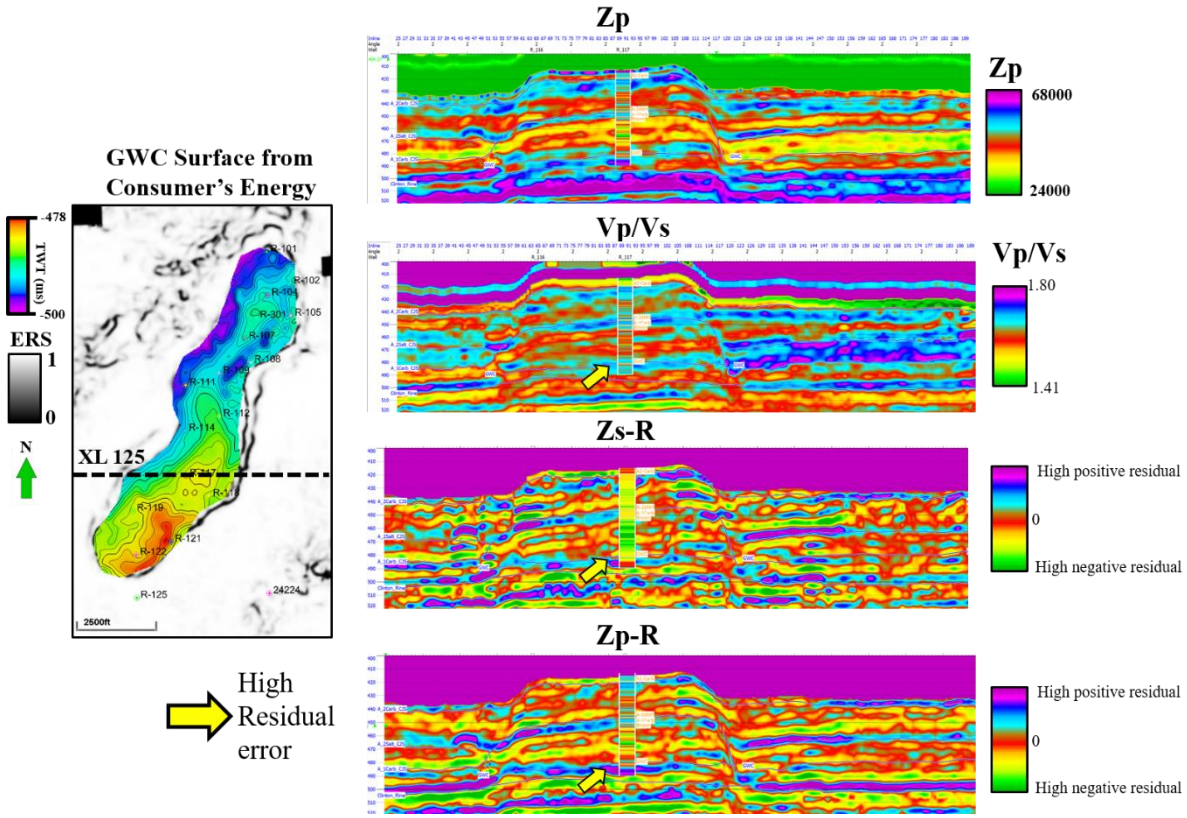

Figure 2.26: Example of high residual error observed in seismic inversion attributes.

Salina Group off of the reef (Figure 2.26). After picking the training polygons, a training data set was produced. In the workflow used, the polygons are used to extract data points (voxels) from the desired input attributes. Seven attributes were used as input for the training data and subsequent exhaustive search: Zp, Zp-R, VpVs-R, Vp, Vp-R, Vs-R, and Vs. These attributes were selected as they all exhibit anomalous values at the approximate GWC (Figure 2.26). An exhaustive search of the training data was done to identify the optimal combination of attributes and their respective smoothing parameter, σ which return the lowest error, E. The combination of Vp-R, Vp, VpVs, Vs-R, Zp with a sigma of 1.5 were found to return the best average error of 0.097. With the PNN model trained, it was then applied to the seismic dataset (Figure 2.27). The time interval was limited to just above and below where the GWC is believed to be, over a

window of 464-500 ms TWT. This was done to avoid misclassification of the overlying A-2 Anhydrite as GWC, as they have a similar expression in the attributes used (Figure 2.26). The PNN classification returns a patchy, but fairly continuous result of the GWC facies within the lower portion of the reef (Figure 2.27).

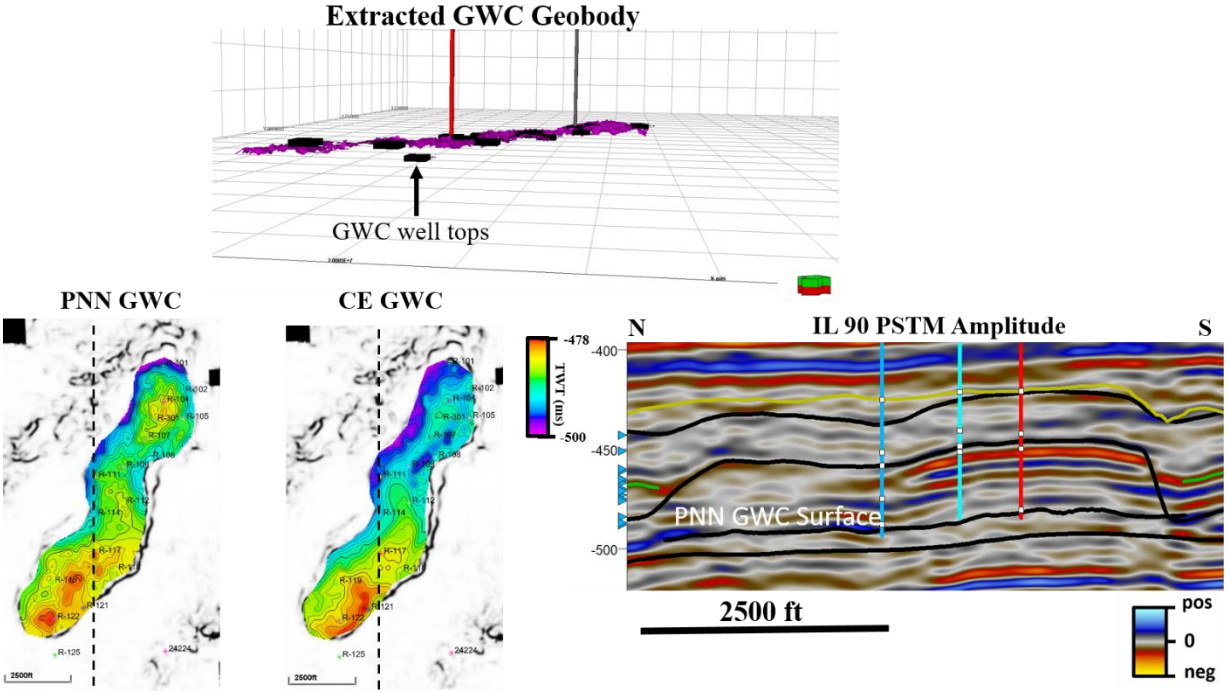

Figure 2.27: Top: Geobody extraction of PNN classified GWC voxels. Left: comparison of PNN GWC surface and the GWC surface provided by Consumer's Energy. Right: Seismic amplitude display of IL 90 with PNN GWC surface displayed. The PNN GWC surface cross cuts amplitudes and has less TWT relief than the CE GWC.

Almost all of the classified voxels are constrained within the reef, with minimal classifications outside. It also appears to cross-cut seismic amplitude reflectors when viewed in cross-section, supporting the claim that interpreting the GWC from amplitude would not be feasible. Using the classified SEG-Y volume output from the classification, a geobody is extracted to enhance the 3-D visualization of the GWC (Figure 2.27). A PNN GWC surface is then created via draping a horizon over the top of the geobody and compared to the initial GWC surface provided by Consumer's Energy (Figure 2.27). The two are remarkably similar, with the PNN GWC surface

having slightly less structural relief than the initial (Figure 27). While the GWC contact was previously known in Ray Reef, this validated workflow can be applied to other Niagaran reefs within the Michigan Basin with seismic surveys available.

3.2: Salt Classification

A second analysis using PNN's was done to classify the A-2 Salt and the carbonate lithologies. In the PSTM amplitude data, the A-2 Salt is characterized by coherent, planar reflectors that are consistent throughout the survey (Figure 2.28). The top of the A-2 Salt

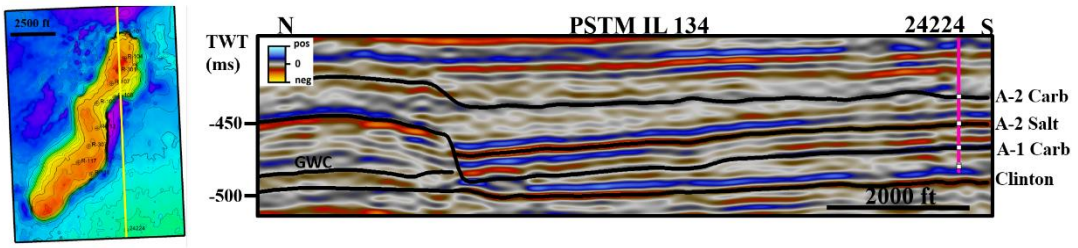

Figure 2.28: Vertical seismic display through the PSTM amplitude data displaying the planar, dim seismic character of the A-2 Salt.

correlates strongly with a negative amplitude (decrease in acoustic impedance) and is easily mapped throughout the survey. Pre-stack inversion attributes greatly enhance the visualization of the A-2 Salt from the encasing carbonate lithologies, as it is represented by low Zp and Vp values as discussed in Investigation 1. The motivation for this analysis is to investigate how PNN classification of evaporite deposits done by supervised machine learning compares to the user classification done in the conventional crossplot analyses. A similar workflow was followed as in Investigation 3.1, and training polygons were picked every 15 lines for both inline and crosslines for both the A-2 Salt and carbonate lithologies (i.e. "Not Salt"). An exhaustive search was done to determine the optimal combination of attributes and sigmas. The combination of the Vp, VpVs, Zp and Zs attributes with a sigma of 0.5 was found to produce the best average error of 0.037. With an optimal suite of attributes and sigma value, the PNN was trained and applied to

the data set (Figure 28).

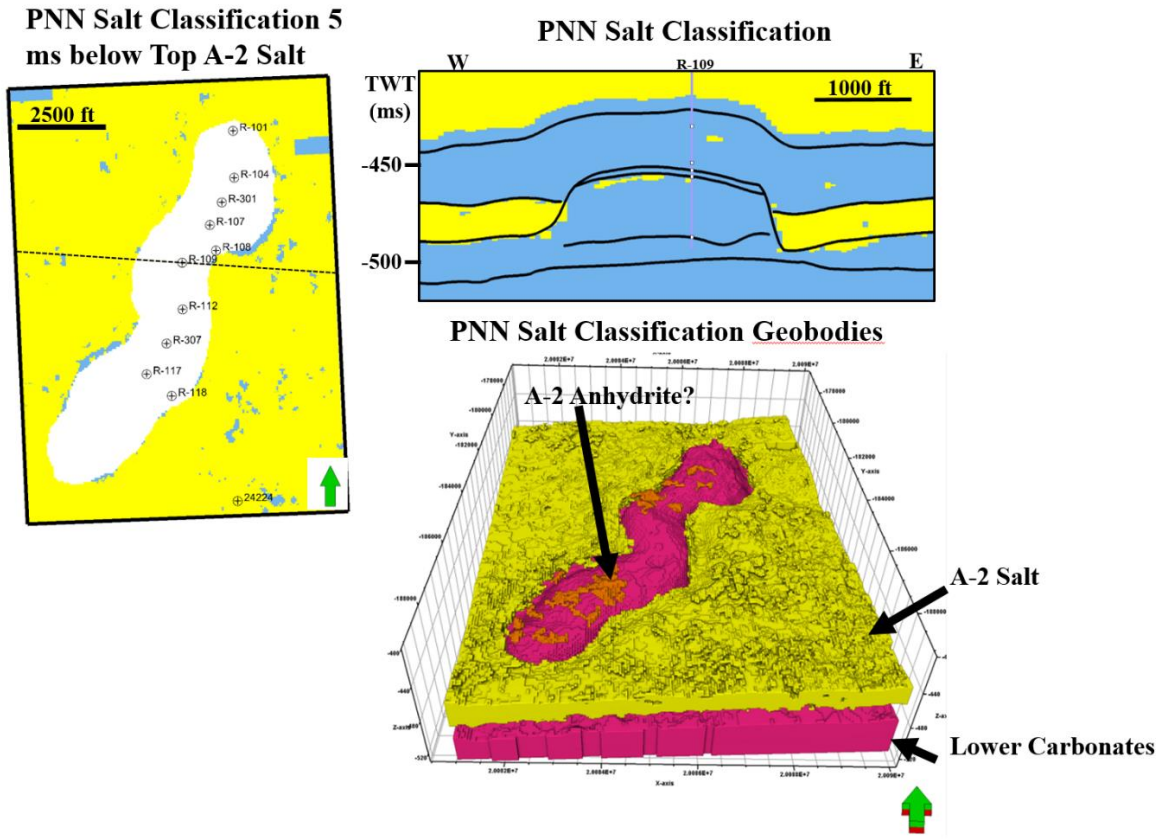

Figure 2.29: Overview of the PNN Salt classification. In the horizon slice, minor patches of misclassifications are present, but overall the salt is correctly classified. Geobody extraction of the salt and not-salt seismic facies accurately captures the morphology of the reef complex.

Minor misclassifications are apparent within the resulting facies volume (Figure 29). Overall the classified salt facies correlate well with the mapped surfaces mapped from the PSTM amplitude data. Geobody extractions of the classified salt and carbonate units with at least 75% confidence accurately capture the morphology and structure of the reef complex and A-2 Salt. The capping A-2 Anhydrite is partially identified as well, as the extraction resulted in a patchy distribution of salt above the reef complex (Figure 2.29).

Discussion

Lithology from Seismic Data

Attempts to derive lithological information from seismic data was a key aspect of this research. A common observation in this study among all the methods was that fine scale variations were not able to be resolved, while larger scale trends were. The deterministic inversion method used provides a "best fit" result, and the resulting inversion models likely do not honor the heterogeneities present within the dolomite reservoir that have been observed in outcrops of other dolomite reservoirs and from core (Hirstius, 2003; Pranter et al., 2005, Haynie 2009; Trout 2012). Insufficient wells with both sonic and density logs and the complete lack of shear logs results prevented the use of stochastic inversion methods that would honor this heterogeneity. Nonetheless, quantitative interpretations were possible utilizing a traditional $\lambda\rho$-$\mu\rho$ analyses (Figure 2.16). Of the methods attempted, this produced the best correlations to well data. The classified seismic facies correlate well with cored well locations, however there is no clear correlation with AAOF data (Figure 2.6, Figure 2.16). While high porosity is typically accompanied by good permeability in Ray Reef (Wold 2008; Haynie 2009), there may be other factors influencing well performance. The unsupervised GTM classification results correlated with the peritidal facies and reef core facies the best, however neither of the distal or proximal aprons could be correlated to core data (Figure 2.21). Qualitatively, from the pre-stack inversion attributes (mainly P-impedance), depositional environments could be interpreted identifying similar geometries from Rine et al.'s (2017) geologic model. In order to see similar geometries, a cross-section perpendicular to the reef's strike provides the best visualization for interpretation (Figure 2.13). Anomalously low Zp values observed in this section could likely be related to karsting caused by subaerial exposure (Wold 2008). These are important facies to be able to

identify, as the windward talus deposits and exposure surfaces are commonly found to have high porosity and permeability values.

Supervised seismic facies classification excelled at more broad classifications of lithology utilizing pre-stack inversion attributes, like salt vs. carbonate (Figure 2.29). Fine-scale classifications of HFU's were not feasible in this particular data set due to the poor time-to-depth relationship and the resolution of the seismic data. Salt classification in Ray Reef was best achieved via crossplotting of inversion attributes and translating well-log relationships to the seismic data (Figure 2.9; Figure 2.16). The PNN did correctly identify the GWC in Ray Reef field utilizing residual inversion attributes. Further analysis needs to be done to understand if this was a user-induced misfit of the GWC during the inversion process, or if there is an observable amplitude anomaly caused by the GWC.

Reservoir Characterization from Seismic Data

One of the goals this study sought to address was to analyze the spatial distribution of reservoir properties from seismic data. This goal was hindered by the lack of shear, sonic and density logs within Ray Reef. Despite the lack of measured wells, the methods used to estimate logs resulted in a good stable pre-stack inversion. Transforming inversion attributes (Zp, Zs) into $\lambda\rho$-$\mu\rho$ volumes allowed for easier estimation of porosity from seismic data (Figure 2.16). This workflow could be valuable to apply to other pinnacle reef reservoirs with pre-stack data available, as zones with favorable reservoir conditions were identified. Comparing the results to well-based geostatistical models, the $\lambda\rho$-$\mu\rho$ classified volume provides a smoother model that has characteristics of the sequence stratigraphic approach by Wold (2008) and the petrofacies approach of Haynie (2009). The classified porosity volume can serve as a valuable probability volume input for future petrophysical models of Ray Reef. The GTM unsupervised classification

provided an estimate of reservoir thickness directly from post-stack seismic attributes. This is a valuable tool as with the consistent spatial distribution of porous reservoir rock observed in Ray Reef (Haynie, 2009), reservoir thickness will have a big impact on well performance as seen with the correlation with AAOF (Figure 2.21). PNN's failed at predicting HFU's and other key reservoir properties directly from seismic in Ray Reef. This is attributed to the poor TDR and relationships of input attributes to the desired logs (Figure 2.23). Being able to predict HFU's directly from seismic data would allow for direct interpretation of well performance from seismic data, which would be an invaluable asset during well planning or monitoring. For this reason, this method should be tried on a pinnacle reef data set with a robust time-depth relationship available (i.e. VSP's, checkshots, shear logs, etc.).

Pitfalls and Best Practices

This study followed several standard assumptions, but interpreters must be aware of the pitfalls associated with any assumptions. The first pitfall, which has been discussed previously, is the basic TDR used in some of the cored wells, and wells with no sonic or density log available. By using a shared or interpolated TDR from seismic horizons to formation tops, possible effects from anisotropy and attenuation due to gas are not accounted for. Moreover, the total depth of every well was not accurately tied to a definite seismic horizon. The stretch/squeezing of reflectors can dramatically affect porosity and permeability logs' positions in cross-section, which ultimately influences the classification of seismic facies using the core data overlay as a guide.

Another pitfall that is difficult to know in legacy fields such as Ray Reef, is whether or not there are fluid/gas effects on measured logs. Sonic logs are heavily affected by the presence of gas (Chopra and Castagna, 2014). Density logs are affected as well, but to a lesser extent. This

unknown can cause errors which carry throughout the study. For example, if an attenuated sonic log was used for density estimation, that will underestimate density. In turn, the calculated P-impedance, calculated shear log, and influence on the seismic inversion low frequency model will be contaminated by the attenuated sonic log. Valid, but simple log estimation was also done in this study (Gardner's relationship). While other methods exist, no wells within the reservoir had both sonic and density logs to analyze the variations imposed by different methods.

Future Work Recommendations

Ray Reef still has a lot of unanswered questions. One area of interest not investigated in this study was rock physics modeling. A comprehensive rock physics analyses would serve as a strong link between the geology, seismic inversion and the petrophysical logs. For instance, it was not apparent the effect dolomitization had from this study. The three previous studies over Ray Reef also had this question remaining (Wold, 2008; Haynie 2009; Trout 2012). Limited analyses have been done on the rock fabrics and pore structures on the microscopic scale for dolomitized pinnacle reefs in Michigan Basin, and travel restrictions prevented such analyses being done for this study. A robust rock physics understanding could also allow for more advanced inversion techniques, such as geostatistical inversion (Vernengo et al., 2014) and other stochastic methods. This would greatly improve the inversion result, as stochastic methods better represent the heterogeneity imposed by the dolomitization of the reef in addition to provide a measure of uncertainty (Haynie, 2009).

Understanding the TDR with more certainty is a valuable undertaking. Whether that is done through additional logging of Ray Reef, or applying neural networks trained on other southern trend reefs to predict missing logs within Ray Reef, that can greatly improve the understanding of Ray Reef from seismic data. Doing so could allow for fine-scale mapping of

horizons in Ray3D, such as the base of the reef (Lockport Formation; “Gray Niagaran”), and onlapping units such as the A-0 Carbonate and Rabbit Ears Anhydrite not considered in this study. These seismic-constrained horizons could then be used as input to constrain future reservoir modeling studies.

Chapter 3: Conclusions

1. Seismic facies were classified from seismic data using a variety of data-driven approaches that incorporated in-context interpretation through crossplotting of seismic attributes. The λρ-μρ crossplot workflow identified zones of good, fair and poor porosity within Ray Reef. Due to the deterministic inversion method, these results may not honor the heterogeneity present in the reservoir, however the large scale trends in porosity distribution were accurately captured within the reef reservoir from seismic data. A consistent distribution of good to fair porosity facies were observed in vertically stacked layers. This is consistent with Wold's (2008) and Haynie's (2009) findings. Future work incorporating stochastic methods have potential to improve these findings. Facies-based inversion could also constrain the results to honor the high degree of heterogeneity present in carbonate lithologies (i.e. Sams et al., 2017). It is observed that areas with higher storage capacity exhibit better measured well flow performance.
2. Unsupervised machine learning applied to post-stack seismic attributes identified the reef core and capping peritidal facies within Ray Reef. It struggled to differentiate the bioherm and apron facies. Future studies should investigate other attribute combinations, in addition to other unsupervised classification methods. This study utilized a literature search to select promising attributes, however no statistical analyses was done on the selected attributes. Statistical methods such as those used in Chenin (2020) for optimal attribute suites may provide better results. Qualitative interpretation of P-Impedance derived from pre-stack inversion can provide direct insight of depositional facies when used in conjunction with Rine et al's (2017) core-based geologic model.

3. Supervised machine learning methods excelled at delineating salt vs. carbonate lithologies in Ray3D. Geobody extraction of these results can potentially serve as input for geocellular modeling from seismic data. HFU estimation using a variety of supervised neural networks from seismic data was unsuccessful in this study, but has potential for success in future studies with robust time-depth and rock physics relationships.
4. Workflows were trialed on one dataset. Future work should apply successful workflows demonstrated herein, such as $\lambda\rho$-$\mu\rho$ and GTM classification, to other nearby southern trend reefs. Shear log prediction was unable to be robustly validated in this study, and future pre-stack inversions should investigate alternative shear wave predictions.

Acknowledgements

This study was made possible through the funding of the Attribute-Assisted Processing & Interpretation (AASPI) consortium sponsors and the Subsurface Detective Agency (SDA). Consumers Energy kindly donated all available seismic and well data used. Sterling Geophysical assisted this study by providing conditioned pre-stack gathers used for seismic inversion. Thanks to Sound-QI for the software licenses for the crossplotting software used, QI-Pro. Enhanced visualization was made possible through Schlumberger for Petrel license donations, and seismic inversions were made possible by CGG for Hampson-Russell license donations.

Appendix A: Pre-stack Inversion parameters

In this appendix, figures are provided of the data input into the pre-stack seismic inversion. The low frequency model used in this study was generated using three wells: Wells 24224, R-117, and R-122. 24224 was chosen as it had measured sonic and density logs, and provided control for off-reef lithologies. R-117 was chosen as it had a measured sonic log and calculated density log. R-122 was chosen as it had a measured density log and calculated sonic log, and provided control for facies located along the reef margin. Horizons used in constructing the low frequency model are: the A-2 Carbonate, A-1 Carbonate, A-2 Salt, and Clinton Formation. Where horizons intersect, the low frequency model was designated to handle truncated and pinch out of layers (i.e. where the A-2 Salt pinches out against the A-1 Carbonate horizon). A 30 sample median filter was applied to the model following lateral interpolation. This filter honored the vertical and lateral contrast, and provided the least amount of interopolation artifacts in the model. The inverse distance power option in HampsonRussel was used for lateral interpolation of well log data. To determine the optimal number of iterations to use in the inversion, a test was done to analyze the error vs. iteration relationship. The resulting plot suggests that 4 iterations provides the optimal minimal error.

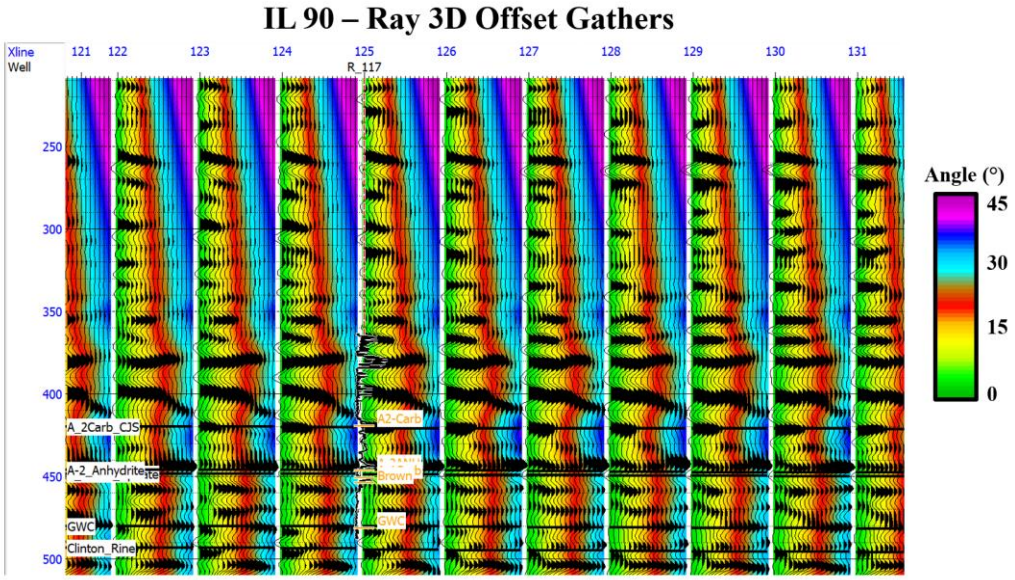

Figure A.30: Conditioned offset gathers as received from Sterling Geophysical colored by angle using a simple velocity model from available sonic logs.

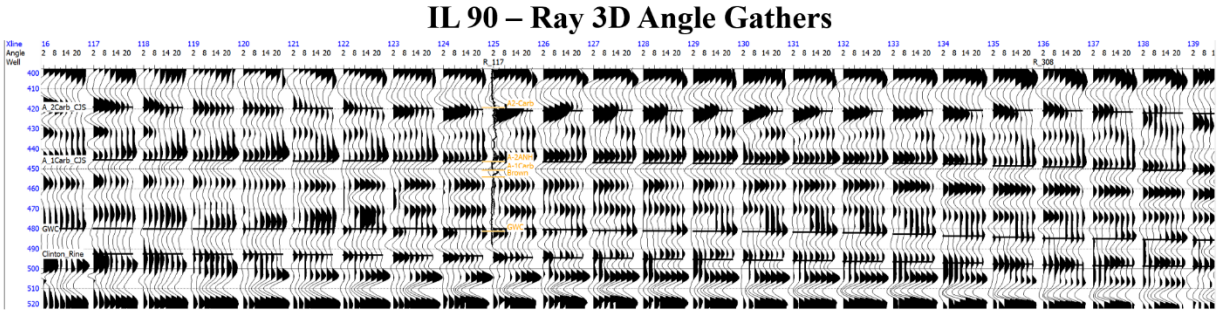

Figure 31: Angle gathers used for pre-stack seismic inversion. Minor trace statics were applied to flatten reflectors, and an angle mute were applied for angles greater than 25 degrees. The volume was cropped to the interval of interest to enhance computation time.

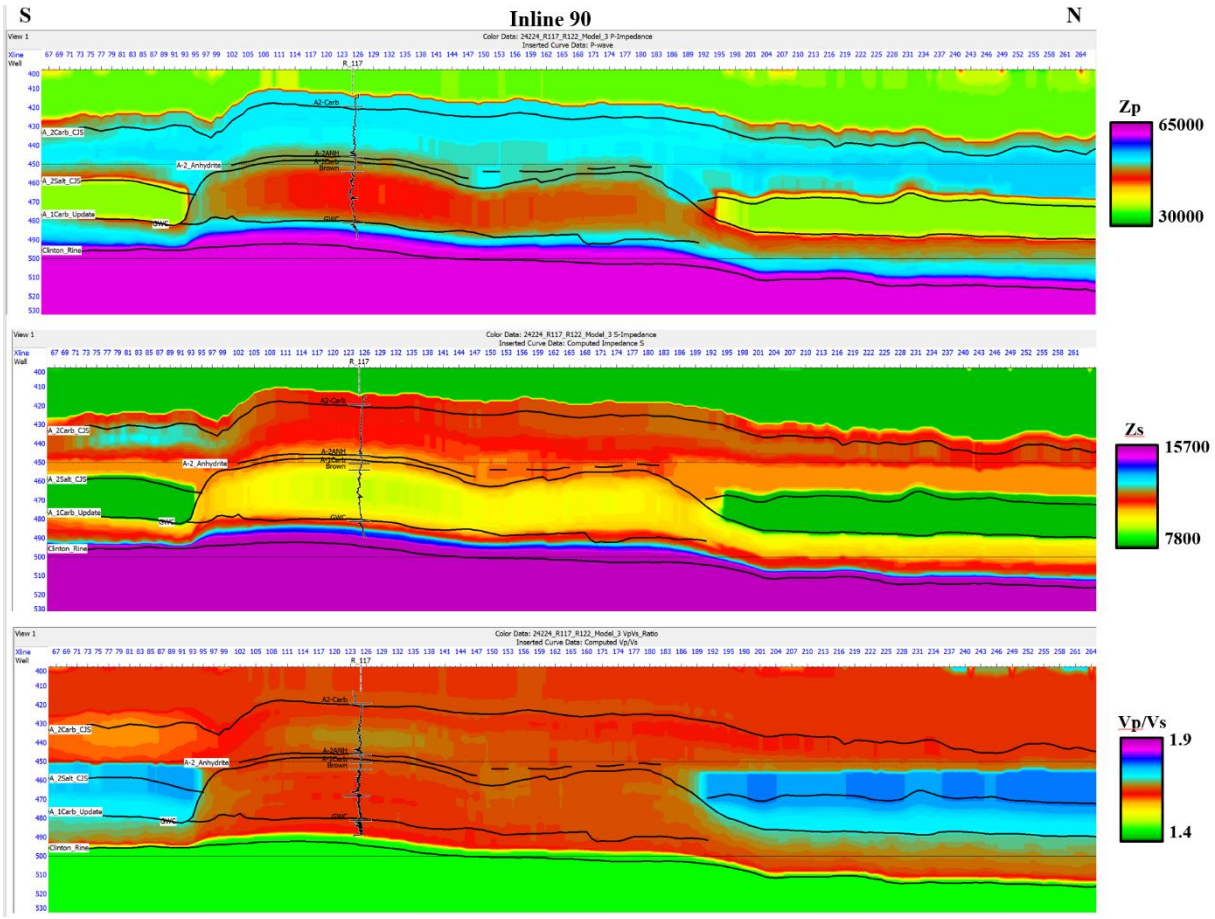

Figure A.32: Cross sections through the low frequency models used in the pre-stack seismic inversion.

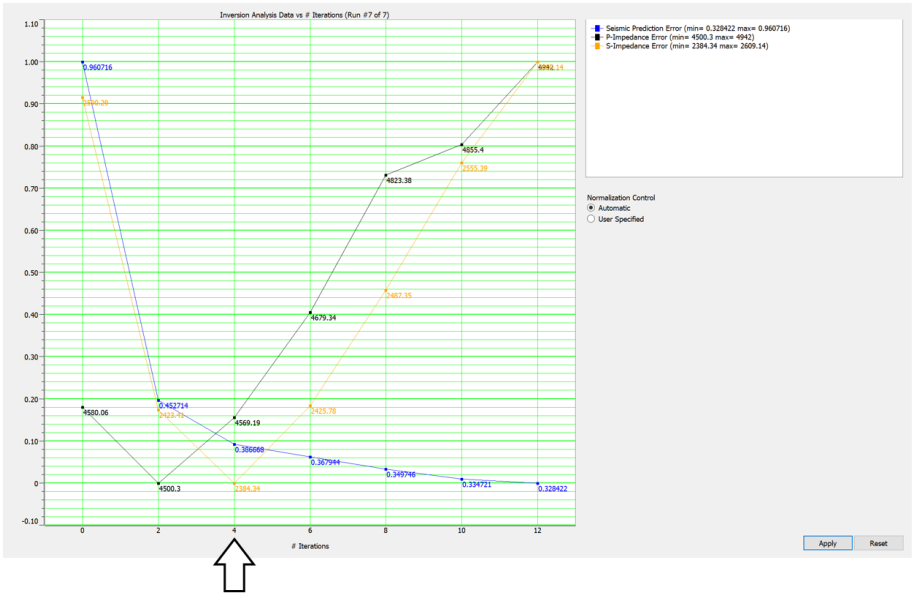

Figure A.33: Pre-stack inversion analysis for the optimal number of iterations. Note after 4 iterations, error for P and S-impedances increase.

References

Aki, K., & Richards, P. G. (1980). *Quantitative seismology*. Freeman.

Amaefule, J. O., Altunbay, M., Tiab, D., Kersey, D. G., & Keelan, D. K. (1993). Enhanced Reservoir Description: Using Core and Log Data to Identify Hydraulic (Flow) Units and Predict Permeability in Uncored Intervals/Wells. *All Days*. https://doi.org/10.2118/26436-ms

Armstrong, D.K., & Carter, T.R. (2010). The subsurface Paleozoic stratigraphy of southern Ontario. Ontario Geological Survey, Special Volume 7, 301p

Barnes, A., 2016, Handbook of Poststack Seismic Attributes: Geophysical References Series, 21, The Society of Exploration Geophysicists, Chapter 4, pages 47-48

Weston Bellman, L. M. (2018). Integrated shale-gas reservoir characterization: A case study incorporating multicomponent seismic data. *Interpretation*, *6*(2). https://doi.org/10.1190/int-2017-0169.1

Bishop, C. M., Svensén, M., & Williams, C. K. (1998). GTM: The Generative Topographic Mapping. *Neural Computation*, *10*(1), 215-234. doi:10.1162/089976698300017953

Briggs, L. I., and D. Briggs, 1974, Niagara-Salina Relationships in the Michigan Basin, Silurian Reef-Evaporite Relationships, Michigan Basin Geological Society Field Conference, Michigan Basin Geological Society, p. 1-23.

Buist, C. R. (2020). *Sub-seismic reef characterization using machine learning and multi-attribute analysis* (Masters dissertation). University of Oklahoma.

Castagna, J. P., and M. M. Backus, 1993, Offset-dependent reflectivity — Theory and practice of AVO analysis: SEG Investigations in Geophysics No. 8, http://dx.doi.org/10.1190/1.9781560802624.

Catacosinos, P.A., P.A. Daniels, and W.B. Harrison, 1991. Structure, stratigraphy, and petroleum geology of the Michigan Basin, in Interior Cratonic Basins: American Association of Petroleum Geologists Memoir 51, p. 561-601.

Catacosinos, P. A., Harrison, W. B., Reynolds, R. F., Westjohn, D. B., & Wollensak, M. S. (2001). Stratigraphic Lexicon for Michigan. Mi DEQ Geology division and Mi Basin Geologic Society. *Bulletin*, *8*, 18-19.

Chenin, J. (2020). Examining Seismic Amplitude Responses of Gaseous Media Using Unsupervised Machine Learning (Masters thesis, University of Oklahoma).

Chopra, S., & Castagna, J. P. (2014). *AVO.* Soc. of Exploration Geophysicists.

Chopra, S. and K. Marfurt, (2005) *Seismic attriubtes – a historical perspective*, Geophysics, 70, 3SO-28SO

Chopra, S., & Marfurt, K. (2006). Seismic Attributes–a promising aid for geologic prediction. *CSEG Recorder*, *31*, 110-120.

Dezfoolian MA, Riahi M Ali, Kadkhodaie-Ilkhchi A (2013) Conversion of 3D seismic attributes to reservoir hydraulic flow units using a neural network approach: an example from the Kanganand Dalan carbonate reservoirs, the world's largest non-associated gas reservoirs, near the Persian Gulf. Earth Sci Res J17(2):75–85

Fatti, J. L., G. C. Smith, P. J. Vail, P. J. Strauss, and P. R. Levitt, 1994, Detection of gas in sandstone reservoirs using AVO analysis: A 3-D seismic case history using the geostack technique: Geophysics, 59, no. 9, 1362–1376, http://dx.doi.org/10.1190/1.1443695

Gardner, G. H. F., L. W. Gardner, and A. R. Gregory, 1974, Formation velocity and density — The diagnostic basics for stratigraphic traps: Geophysics, 39, no. 6, 770–780, http://dx.doi.org/10.1190/1.1440465.

Gassmann, F., 1951, Über die Elastizität poroser Medien [On elasticity of porous media]: Vierteljahrsschrift der Naturforschenden Gesellschaft in Zürich, 96, 1–23.

Gill, D., 1977, The Belle River Mills Gas Field: Productive Niagaran Reefs Encased by Sabkha Deposits, Michigan Basin: Michigan Basin Geological Society, Special Papers No. 2, 188 p.

Goodway, W., J. Varsek, and C. Abaco, 2006, Practical applications of P-wave AVO for unconventional gas resource plays, part 2: Detection of fracture prone zones with azimuthal AVO and coherence discontinuity: CSEG Recorder, 31, no. 4, 52–65, http://209.91.124.56/publications/recorder/2006/04apr/apr2006-p-waveavo.pdf,

Goodway, B., T. Chen, and J. Downton, 1997, Improved AVO fluid detection and lithology discrimination using Lamé petrophysical parameters; "$\lambda\rho$", "$\mu\rho$", & "λ/μ fluid stack" from P and S inversions: 67th Annual International Meeting, SEG, Expanded Abstracts, 183–186, http://dx.doi.org/10.1190/1.1885795

Grammer, G. M., D. A. Barnes, W. B. Harrison III, A. E. Sandomierski, and R. G.Mannes, 2009, Practical synergies for increasing domestic oil production and geological sequestration of anthropogenic CO2: An example from the Michigan Basin, in M. Grobe, J. C. Pashin, and R. L. Dodge, eds., Carbon dioxide sequestration in geological media—State of the science: AAPG Studies in Geology 59, p. 689–706

Hajmeer, M., & Basheer, I. (2002). A probabilistic neural network approach for modeling and classification of bacterial growth/no-growth data. *Journal of microbiological methods*, *51*(2), 217-226.

Hampson, D. P., B. H. Russell, and B. Bankhead, 2005, Simultaneous inversion of pre-stack seismic data: 75th Annual International Meeting, SEG, Expanded Abstracts, 1633–1638, http://dx.doi.org/10.1190/1.2148008.

Harvey, P. J., 1993, Porosity identification using AVO in Jurassic carbonate, offshore Nova Scotia: The Leading Edge, 12, 180–184. http://dx.doi.org/10.1190/1.1436940.

Haynie, Jill M. (M.S. Geology [Department of Geological Sciences]) 2009. Characterization and modeling of petrofacies and pore-volume distribution within a gas-storage reservoir, Ray Reef Field, Southern Michigan Basin, Michigan. Thesis directed by Associate Professor Matthew J. Pranter

Hilterman, F. J. and R.W. Verm, 1994, Lithologic color-coded sections by AVO crossplots:64th Annual International Meeting, Society of Exploration Geophysicists Expanded Abstracts, 1092-1095.

Hirstius, C.B., 2003. Multiple scales of lateral petrophysical heterogeneity within dolomite lithofacies as determined from outcrop analogs: Implications for 3-D modeling. Master thesis, University of Colorado, Boulder, 160 p.

Hoffe, B. H., M. A. Perez, and W. Goodway, 2008b, AVO interpretation in LMR space: A primer: Presented at the CSPG/CSEG/CWLS Annual Convention, http://www.cspg.org/documents/Conventions/Archives/Annual/2008/237.pdf

Howell, Paul D., and Ben A. Van Der Pluijm. "Structural Sequences and Styles of Subsidence in the Michigan Basin." *Geological Society of America Bulletin* 111.7 (1999): 974-91. Print.

Howell, Paul D., and Ben A. Van Der Pluijm. "Early History of the Michigan Basin: Subsidence and Appalachian Tectonics." *Geology* 18.12 (1990): 1195. Print.

Huh, J. M., L. I. Briggs, and D. Gill, 1977, Depositional Environments of Pinnacle Reefs, Niagara and Salina Groups, Northern Shelf, Michigan Basin, *in* American Association of Petroleum Geologists, ed., Reefs and Evaporites - Concepts and Depositional Models:Studies in Geology, v. 5: Tulsa, American Association of Petroleum Geologists, p. 1-21.

Seismic imaging in and around salt bodies Jones, Ian F. et al. Interpretation (2014),2(4): SL1http://dx.doi.org/10.1190/INT-2014-0033.1

Jodry, R. L., 1969, Growth and dolomitization of Silurian reefs, St. Clair County, Michigan. American Association of Petroleum Geologists Bulletin, v. 53, p. 957-981.

Liebold, A. W., III, 1992, Sedimentological and geochemical constraints on Niagaran/Salina deposition, Michigan basin [Ph.D. thesis]: Ann Arbor, University of Michigan, 280 p.

Li, Y., J. Downton, and W. Goodway, 2003a, Recent applications of AVO to carbonate reservoirs in the Western Canadian Sedimentary Basin: The Leading Edge, 22, no. 7, 670–674, http://dx.doi.org/10.1190/1.1599694.

Lubo-Robles, D., Ha, T., Lakshmivarahan, S., Marfurt, K. J., & Pranter, M. J. (2021). Exhaustive probabilistic neural network for attribute selection and supervised seismic facies classification. *Interpretation*, *9*(2), T421-T441.Mahmoud et al., 2009

Masters, T., 1995, Advanced algorithms for neural networks: John Wiley & Sons

Maurya, S. P., & Sarkar, P. (2016). Comparison of post stack seismic inversion methods: a case study from Blackfoot Field, Canada. *International Journal of Scientific and Engineering Research*, *7*(8), 1091-101.

Mesolella, K. J., J. D. Robinson, L. M. McCormick, and A. R. Ormiston, 1974, Cyclic Deposition of Silurian Carbonates and Evaporites in Michigan Basin: American Association of Petroleum Geologists Bulletin, v. 58, p. 34-62.

Mood and Graybill, 1962 A.M. Mood, F.A. Graybill Introduction to the theory of statistics Macmillan, New York (1962)

Nejad, M. R. S., Hassani, H., Khorasani, M. M., Javaherian, A., and M. R. Sokooti, 2009, The investigation of the spectral decomposition application in detecting reef reservoir on Abadan Plain, Iran, Australian Journal of Basin and Applied Sciences, 3(2), 866-874

Ostrander, W. J., 1982, Plane wave reflection coefficients for gas sands at nonnormal angles of incidence: 52nd Annual International Meeting, SEG, Expanded Abstracts, 216–218, http://dx.doi.org/10.1190/1.1826898.

Pedregosa *et al.*, Scikit-learn: Machine Learning in Python JMLR 12, pp. 2825-2830, 2011.

Prasad, M. (2003). Velocity-permeability relations within hydraulic units. Geophysics. 68: 108-117.

Rine, Matthew. (2015). Depositional Facies and Sequence Stratigraphy of Niagaran-Lower Salina Reef Complex Reservoirs of the Guelph Formation, Michigan Basin. 10.13140/RG.2.2.20337.79203.

Rine, M. J., J. D. Garrett, and S. E. Kaczmarek, 2017, A New Facies Architecture Model For the Silurian Niagaran Pinnacle Reef Complexes Of The Michigan Basin: Characterization and Modeling of Carbonates–Mountjoy Symposium 1, doi:10.2110/sepmsp.109.02.

Rine, M. J., McLaughlin, P. I., Bancroft, A. M., Harrison III, W. B., Kuglitsch, J., Caruthers, A. H., ... & Emsbo, P. (2020). Linked Silurian carbon cycle perturbations, bursts of pinnacle reef growth, extreme sea-level oscillations, and evaporite deposition (Michigan Basin, USA). *Palaeogeography, Palaeoclimatology, Palaeoecology*, *554*, 109806.

Roksandic, m. M. (1978). Seismic facies analysis concepts. *Geophysical Prospecting*, *26*(2), 383–398. https://doi.org/10.1111/j.1365-2478.1978.tb01600.x

Roy, A. (2013). *Latent Space Classification of Seismic Facies* (Doctoral dissertation). University of Oklahoma.

Saadatinejad, M. R., Javaherian, A., and K. Sarkarinejad, 2012, Investigation of the various spectral decomposition methods to detect and explore hidden complex reef reservoir structures and their hydrocarbon potentials in northwestern part of the Persian Gulf, Energy Exploration & Exploitation, 30(6), 867-888

Sams, Mark, Paul Begg, and Timur Manapov. (2017)"Seismic Inversion of a Carbonate Buildup: A Case Study." *Interpretation* 5.4. Print.

Scotese, C.R., 2002, Paleomap http://www.scotese.com/

Sears, S. O., and F. J. Lucia, 1979, Reef-growth model for Silurian pinnacle reefs, northern Michigan reef trend: Geology, v. 7, p. 299-302.

Shier, D.E., 1991. Textbook on Well Log Normalization. Englewood, CO: Energy Data Services. Sleep et al., 1980

Specht, D. F. (1990). Probabilistic neural networks. *Neural Networks*, *3*(1), 109–118. https://doi.org/10.1016/0893-6080(90)90049-q

Taner, 1978, Taner, M. T., 1978, Complex seismic trace analysis: Geophysics, 44, 1041–1063.

Tellez, J., Pranter, M. J., Sondergeld, C., Rai, C., Fu, J., Han, H., ... & McLain, C. (2021). Mechanical stratigraphy of Mississippian strata using machine learning and seismic-based reservoir characterization and modeling, Anadarko Basin, Oklahoma. *Interpretation*, *9*(2), SE53-SE71.

Toelle, B. and Y. V. Ganshin, 2018, Porosity characterization in a Silurian reef, northern Michigan Basin, using azimuthal seismic data and potential impacts for enhanced oil recovery, The Geological Society of America, Special Paper 531, 157-173

Trout, J. L. (2012). Faunal Distribution and Relative Abundance in a Silurian (Wenlock) Pinnacle Reef Complex-Ray Reef, Macomb County, Michigan.

Vernengo, L., Czeplowodzki, R., Trinchero, E., Sabaté, A., Tsybulkina, I., & Morillo, F. (2014). Improvement of the reservoir characterization of fluvial sandstones with geostatistical inversion in Golfo San Jorge Basin, Argentina. *The Leading Edge*, *33*(5), 508-518.

Wang, Z., 1997, Seismic properties of carbonate rocks, *in* I. Palaz and K. J. Marfurt, eds., Carbonate seismology: SEG Geophysical Developments Series No. 6,29–52, http://dx.doi.org/10.1190/1.9781560802099. ch3.

White, R. E., 1991, Properties of instantaneous seismic attributes: The Leading Edge, 10, no. 07, 26-32. (Discussion and reply in TLE-11-8-45-46 and TLE-11-10-10-12

Wold, J., 2008, Sequence Stratigraphy and 3-D Reservoir Characterization of a Silurian (Niagaran) Reef – Ray Gas Storage Field, Macomb County, Michigan [Master's Thesis]: Kalamazoo, Michigan, Western Michigan University. 294 p.

Xu, S., Chen, G., Zhu, Y., Zhang, J., Payne, M., Deffenbaugh, M. Dunsmuir, J. H. (2007). Carbonate Rock Physics: Analytical Models and Validations Using Computational Approaches and Lab/Log Measurements. International Petroleum Technology Conference. doi:10.2523/iptc-11308-ms

Zheng, Q., 1999. Carbonate diagenesis and porosity evolution in the Guelph Formation, Southwestern Ontario. Doctoral thesis, University of Waterloo, Waterloo, Ontario, Canada, 281 p.